

Spectral properties and pseudogap in the stripe phases of cuprate superconductors

Marcus Fleck

Max-Planck-Institut für Festkörperforschung, Heisenbergstrasse 1, D-70569 Stuttgart, Federal Republic of Germany

Alexander I. Lichtenstein

University of Nijmegen, Toernooiveld 1, NL-6525 ED Nijmegen, The Netherlands

Andrzej M. Oleś

Institute of Physics, Jagellonian University, Reymonta 4, PL-30059 Kraków, Poland,

and Max-Planck-Institut für Festkörperforschung, Heisenbergstrasse 1, D-70569 Stuttgart, Federal Republic of Germany

(Received 22 February 2001; revised manuscript received 21 June 2001; published 13 September 2001)

Using an exact diagonalization method within the dynamical mean-field theory we analyze the stable stripe structures found in the two-dimensional Hubbard model doped by $0.03 < \delta < 0.2$ holes, and discuss a scenario for stripe melting. Our results demonstrate the importance of dynamical correlations which lead to the metallic stripes, in contrast to the Hartree-Fock picture. The spectral functions show a coexistence of the coherent quasiparticles (polaron band) close to the Fermi energy μ , and incoherent states at lower energies. The quasiparticles in the polaron band depend on hole doping, and hybridize strongly with the partly filled mid-gap band within the Mott-Hubbard gap, induced by stripe order. This explains the origin of nondispersive quasiparticles close to the Fermi energy μ , observed near the $X = (\pi, 0)$ and $Y = (0, \pi)$ points for the samples with coexisting (10) and (01) stripes. We reproduce the gap which opens for charge excitations at the $S = (\pi/2, \pi/2)$ point, observed in the angle-resolved photoemission experiments for $\text{La}_{2-x}\text{Sr}_x\text{CuO}_4$, and a pseudogap in the integrated spectral density pinned to μ . Finally, we show that large spectral weight close to μ moves from the X to the S point when the second neighbor hopping element increases, and the (01) stripe phase is destabilized by kink fluctuations.

DOI: 10.1103/PhysRevB.64.134528

PACS number(s): 74.72.-h, 71.10.Fd, 79.60.-i, 74.20.Mn

I. INTRODUCTION

As one of very few predictions in the theory of high-temperature superconductors (HTS's), *the stripes* were found in Hartree-Fock (HF) calculations on finite lattices described by the Hubbard model,¹ well before their experimental confirmation.² Such states result from the competition between the superexchange interactions which are at maximum in the undoped materials, and the kinetic energy of the holes which is optimized when the density of doped holes in the domain walls is large.^{3,4} This phase separation into a stripe phase is very general and occurs in various transition-metal oxides,^{5,6} but is best explored in the cuprates for several reasons: First of all, better insight into the stripe stability would help to understand whether the stripes support or oppose superconductivity,^{7,8} and thus would contribute to the understanding of the mechanism of high-temperature superconductivity itself. Second, more experimental data were collected for the cuprates so far than for any other class of perovskites, motivated by interest in the novel mechanism of superconductivity in these materials.⁹ Finally, the theoretical models of the cuprates are simpler than those of nickelate or manganite perovskites, as the coupling to the lattice does not induce Jahn-Teller distortions, and other complications such as orbital physics of manganites⁶ are absent.

The undoped compounds, La_2CuO_4 and $\text{YBa}_2\text{Cu}_3\text{O}_6$, are charge-transfer insulators due to strong Coulomb interaction U on Cu ions,⁶ and exhibit long-range antiferromagnetic (AF) order due to superexchange interactions. It is rapidly destroyed and replaced by short-range AF correlations when

holes are doped into the CuO_2 planes.^{10,11} The resulting periodic structure with AF domains separated by one-dimensional (1D) domain walls of nonmagnetic atoms is the simplest realization of the so-called *stripe phase*.¹² One of the mysteries at the early stage of the HF studies of stripe phases was the filling of the domain walls. On one hand, these numerical studies of the Hubbard model showed the domain walls with the filling of one doped hole per domain-wall atom (called *filled stripes*) to be the most stable structures,^{1,13} and indeed the stripes found in the nickelates provide a good example of such filled stripes.^{14,15} On the other hand, the experiments performed on $\text{La}_{1.6-x}\text{Nd}_{0.4}\text{Sr}_x\text{CuO}_4$ are consistent with the filling of one doped hole per two domain-wall atoms (called *half-filled stripes*).² Therefore a natural question arises as to *why the stripes in the cuprates are so different*, and cannot be described just by the HF calculations, performed on the Hubbard^{1,13} or on a charge-transfer (three-band) model.^{15,16}

First attempts to describe the stripes, including their discovery,¹ were made within the single-particle theory, where the local Coulomb interaction U was replaced by the local potentials, determined self-consistently within the HF approximation. It is well known that such potentials stabilize the AF state at half filling ($n=1$), and the electronic structure consists of two Hubbard subbands. A domain wall with nonmagnetic atoms, and uniformly distributed hole density of one hole per two atoms, is unstable in this limit, as it would correspond to a quarter filled band crossing the Fermi level μ , and would therefore give a 1D metallic conductivity along the domain walls. Such metallic states are, of course,

locally unstable in HF, and could be stabilized only by an additional electronic instability which would open a gap at $\omega = \mu$.¹³ Indeed, this kind of instability may occur due to an extra quadrupling of the periodicity along the domain walls, with either alternating charges along the walls, as a charge-density wave (CDW) instability, or with alternating magnetic moments, as a spin-density wave (SDW) instability. This explains the difficulty to stabilize the observed stripe structures with half filled domain walls at doping $\delta = 1/8$, with $\delta = 1 - n$ given by the electron density n . In contrast, a 1D band which originates from the stripe structure becomes empty when a domain wall is filled by one hole per each atom, i.e., for the filled domain wall. As a result, the stripe structures stable in HF are always insulating.

Stripes may be seen as topological defects in an antiferromagnet, stabilized by the kinetic energy of the doped holes.¹⁷ Their stability has a solitonic origin with nonmagnetic domain-wall atoms, as shown both for small clusters,¹³ and for a 1D electron system described by the Hubbard model.¹⁸ This explains why the most stable structures have an integral filling of one hole either per one or per two atoms within the domain wall. Although no evidence was presented yet, it seems that the larger spins $S = 1$ of Ni^{2+} ions and the degeneracy of $3d$ orbitals play a role in stabilizing the filled stripes in the nickelates. In contrast, orbital degeneracy is absent in the cuprates, and the corrections due to electron correlations are particularly large. In fact, it was shown that *they are responsible for stabilizing the half-filled stripes* in these systems.^{19–24} It is easy to understand that the correlation energy has to be larger in the half filled than in the filled stripe phases by analyzing the dependence of correlation energy on the electronic filling.²⁵ The electron density at the domain-wall atoms is larger in the half filled than in the filled stripe structures, and therefore more energy can be gained by reducing the double occupancy in the former phases. Indeed, such corrections beyond the HF states stabilize the half-filled stripe phases, and these structures were determined in the ground state within several techniques: mean-field slave-boson approximation,¹⁹ density-matrix renormalization group (DMRG),²⁰ variational (local ansatz) approach,²¹ quantum Monte Carlo (QMC) calculations,²² and by an explicit analysis of the string configurations.²³ Although the long-range Coulomb interactions might help to stabilize the stripe order,¹⁹ these studies, including our approach which uses the dynamical mean-field theory (DMFT),²⁴ have shown that the on-site interactions alone suffice to obtain stable half-filled stripes.

Experimentally the stripes are observed as the shift of the neutron peak $\propto \eta$, which splits into four peaks away from the AF maximum at $\mathbf{Q} = (\pi, \pi)$ to the points $\mathbf{Q} = [(1 \pm 2\eta)\pi, \pi]$ and $\mathbf{Q} = [\pi, (1 \pm 2\eta)\pi]$ along the (10) and (01) direction, and depends on hole doping δ .^{2,10,26} This result shows that the stripes in the cuprates are (10) type, in contrast to the diagonal (11) stripes observed in the nickelates.¹⁴ In fact, in the underdoped regime of $\delta < 1/8$, the relation $\eta \approx \delta$ holds, while at $\delta > 1/8$ one finds instead a lock-in effect with $\eta = 1/8$.²⁶ This behavior allows us to conclude that the domain walls have an optimal filling of one hole per two domain-wall atoms, and the size of the AF domains de-

creases under doping as long as $\delta < 1/8$, and the domain walls are not too close to each other. However, the smallest unit cell for a stable (01) stripe phase consists of charge unit cells with four atoms, and thus doping above $\delta = 1/8$ modifies the density distribution within the AF domains, and finally leads to the disappearance of stripes, i.e., stripe melting at $\delta \approx 0.20$. Recently we have demonstrated²⁴ that this behavior can be reproduced within the Hubbard model when the electron correlation effects are treated using the DMFT.²⁷ This method is very powerful as it allows us to treat the leading hole correlations, represented by *local self-energy*,²⁸ both in the ground state and in the excitation spectra. The DMFT analytic approach allows to separate the charge fluctuations at large energy from the spin fluctuations, leading to a very satisfactory description of the Hubbard model at half filling,²⁹ and can be extended to study the stripe phases.³⁰ Apart from the neutron scattering, the stripe phase has also measurable consequences in angle-resolved photoemission (ARPES) spectroscopy, and these may be directly investigated using the single-particle Green function calculated within the DMFT.

The purpose of the present paper is threefold. First of all, we present the evolution of stripe phases under increasing doping, focusing particularly on the low-doping and high-doping regime. Thereby we use an unbiased nonperturbative solution which allows us to achieve a satisfactory accuracy, obtained using the exact diagonalization (ED) method of Caffarel and Krauth to determine the self-energy.³¹ The stripes were observed experimentally at low hole doping $x \approx 0.04$ first as diagonal (11) stripes, and next as vertical (01) stripes, stable in the regime of higher doping $\delta > 0.06$.³² We will show that this crossover is even quantitatively reproduced by the present calculations. At a higher doping $\delta > 1/8$ we investigate the phenomenon of stripe melting, and show that it is related to the competition between the site-ordered and bond-ordered stripe structures, known to be almost degenerate in the HF studies.¹⁶ In fact, these two phases are also not distinguishable experimentally in the neutron scattering, and are both likely to be local energy minima, provided the quantum fluctuations are moderate and do not mix such configurations with each other. The stability of static stripe structures in the DMFT depends on charge fluctuations which might favor the site-ordered structures, and on spin fluctuations, lowering the energy of bond-ordered stripes.⁴ We will concentrate thereby on the generic features of the doped cuprates, and thus investigate primarily the stripe phases using the Hubbard model with only nearest-neighbor hopping. This model is adequate for La-based cuprates,^{33,34} where the quasistatic stripes were observed in samples with and without Nd.^{2,35}

As a second problem we address the spectral properties of stripe phases. Perhaps the best known observations are: (i) a quasi-1D Fermi surface close to $(\pi, 0)$ and equivalent points, (ii) a decreased spectral weight at the Fermi level μ ,³⁶ and (iii) a real gap which opens for charge excitations around momentum $\mathbf{k} = (\pi/2, \pi/2)$, observed in $\text{La}_{2-x-y}\text{Nd}_y\text{Sr}_x\text{CuO}_4$.^{37–39} By analyzing the chemical potential dependence on the doping level δ , Ino *et al.* have shown that the Fermi-liquid picture breaks down in the underdoped

regime.³⁶ Thus the stripe superstructure leads to drastic changes of the spectral weight distribution, as shown by recent theoretical studies.^{7,24,40–44} However, many detailed questions related to the momentum dependence of the photoemission (PES) spectra,⁴⁵ such as (i) the origin of the flat quasiparticle (QP) peak near the $\mathbf{k}=(\pi,0)$ point, (ii) the mechanism of pseudogap observed at the Fermi energy μ , and (iii) the absence of a 1D band at the Fermi energy which could be expected for half-filled domain walls at $\mathbf{k}=(\pi,\pi/4)$ and $\mathbf{k}=(\pi/4,\pi/4)$ points, have to be answered before a consistent interpretation of the ARPES experiments might be formulated. Below we concentrate on the above questions and compare the results of our DMFT calculations with the measured ARPES spectra.

Finally, we consider also the effect of the second neighbor hopping on the stripe phases, and analyze the changes in the spectral properties induced by this element. We determine the energy associated with kinks along the domain walls and show that they are responsible for destabilizing the (01) stripes in Y and Bi compounds, where this hopping element is large.

The rest of this paper is organized as follows. In Sec. II we present the details of the self-consistent problem derived and solved within the DMFT for the stripe phases. The stripe phases obtained for different doping regimes and the melting of stripe ordering above $\delta=0.15$ are discussed in Sec. III. Next the one-particle excitation spectra as obtained for stripe phases are analyzed in Sec. IV. Here we consider such questions as the momentum dependence of the spectral functions, their drastic changes with respect to the HF counterparts, and the modifications of the spectral weight distribution caused by increasing doping. We discuss also the origin of the stripe stability and its relation to the pseudogap. The effect of second-neighbor hopping on the stripe stability and the induced by it changes in the spectral properties are analyzed in Sec. V. Some open questions and our conclusions are presented in Sec. VI.

II. FORMALISM

A. Dynamical mean-field theory for stripe phases

We consider the Hubbard model with on-site Coulomb interaction U ,

$$H = - \sum_{\langle mi,nj \rangle, \sigma} t_{mi,nj} a_{mi\sigma}^\dagger a_{nj\sigma} + U \sum_{mi} n_{mi\uparrow} n_{mi\downarrow}, \quad (1)$$

defined on a two-dimensional (2D) square lattice. In the stripe phase the lattice is covered by N supercells containing L sites each. Positions $\mathbf{R}_{mi} \equiv \mathbf{T}_m + \mathbf{r}_i$ of nonequivalent sites $i=1, \dots, L$ within a given unit cell m are labeled by a pair of indices: $\{mi\}$ and $\{nj\}$, respectively. The CuO_2 planes of HTS's are frequently described by the effective Hubbard model (1) which may be derived from the realistic charge-transfer model either by a cell perturbation method,³³ or by the down-folding procedure in electronic structure calculations.³⁴ Both methods lead to similar results; they have shown that the second-neighbor hopping element t' describes the differences in the electronic structure

between various HTS's, and is small ($-0.1t \lesssim t' < 0$) for $\text{La}_{2-x}\text{Sr}_x\text{CuO}_4$ compounds. Therefore we neglected this element in most of the present study, and we investigate primarily long-range stripe order in the Hubbard model with nearest-neighbor hopping element: $t = t_{mi,nj}$, if pairs $\{mi\}$ and $\{nj\}$ refer to nearest-neighbor sites.

The DMFT treatment of the stripe phases rests on the assumption that the leading charge and spin correlations are local and can thus be described by *local self-energy*.²⁸ Although this assumption is plausible, it can be justified only *a posteriori* by comparing the calculated results with some available rigorous results for a 2D system. In fact, we have shown before that within the DMFT one obtains the correct dispersion and spectral weights of the QP states in the Hubbard model at half filling ($n=1$), if the spin fluctuations are included in the local self-energy.²⁹ Motivated by this success, we have generalized the DMFT method to the geometry of stripe phase, where the local self-energies $\Sigma_{i\sigma}(\omega)$ are labeled by the site index i within a stripe supercell. The method is analogous to that used recently by Potthoff and Nolting for studying the Mott transition in thin films.⁴⁶

The Green's function defined for imaginary time $\tau = it$,

$$G_{mi,nj,\sigma}(\tau) = -\theta(\tau) \langle a_{mi\sigma}(\tau) a_{nj\sigma}^\dagger(0) \rangle + \theta(-\tau) \times \langle a_{nj\sigma}^\dagger(\tau) a_{mi\sigma}(0) \rangle, \quad (2)$$

depends on the supercell indices m and n , on the indices within the supercell i and j , and on the spin index σ . Its Fourier transform $\hat{G}_\sigma(\mathbf{k}, i\omega_\nu)$ is an $(L \times L)$ matrix, obtained using the periodicity of the stripe phase, and the transformation to the fermionic Matsubara frequencies $\omega_\nu = (2\nu + 1)\pi T$, where T is a fictitious temperature playing a role of a low-energy cutoff.²⁷ The elements of its inversion are given by

$$G_{ij\sigma}^{-1}(\mathbf{k}, i\omega_\nu) = (i\omega_\nu + \mu) \delta_{ij} - h_{ij}(\mathbf{k}) - \Sigma_{i\sigma}(i\omega_\nu) \delta_{ij}. \quad (3)$$

Here the site- and spin-dependent *local self-energy*,^{27,28}

$$\Sigma_{i\sigma}(i\omega_\nu) = \Sigma_{i\sigma}^{\text{HF}} + \Sigma_{i\sigma}^{\text{D}}(i\omega_\nu), \quad (4)$$

consists of a HF (static) potential $\Sigma_{i\sigma}^{\text{HF}}$,

$$\Sigma_{i\sigma}^{\text{HF}} = U n_{i,-\sigma}, \quad (5)$$

where $n_{i,-\sigma} = \langle n_{mi,-\sigma} \rangle$ is the average density of $-\sigma$ -spin electrons at site i in a stripe unit cell, and of a dynamic part $\Sigma_{i\sigma}^{\text{D}}(i\omega_\nu)$, which describes local electron correlations. The kinetic energy in Eq. (3) is obtained for the stripe lattice with supercells of L atoms as an $(L \times L)$ matrix $\hat{h}(\mathbf{k})$, and its matrix elements are

$$h_{ij}(\mathbf{k}) = \sum_n \exp[-i\mathbf{k}(\mathbf{R}_{0i} - \mathbf{R}_{nj})] t_{0i,nj}. \quad (6)$$

If the hopping in the Hubbard model (1) is restricted to nearest neighbors only, the summation in Eq. (6) includes only either two sites within the same supercell, or the nearest-neighbor atoms $\{nj\}$ of adjacent stripe supercells.

The local Green's functions $G_{i\sigma}(i\omega_\nu)$ for each nonequivalent site i in the stripe phase are calculated from the diagonal elements of the Green's function matrix (3),

$$G_{i\sigma}(i\omega_\nu) = \frac{1}{N} \sum_{\mathbf{k}} G_{ii\sigma}(\mathbf{k}, i\omega_\nu). \quad (7)$$

The DMFT equations lead then to a self-consistent problem at site $i = 1, \dots, L$,²⁴

$$\mathcal{G}_{i\sigma}^{-1}(i\omega_\nu) = G_{i\sigma}^{-1}(i\omega_\nu) + \Sigma_{i\sigma}(i\omega_\nu), \quad (8)$$

where $\mathcal{G}_{i\sigma}(i\omega_\nu)$ is the effective medium (bath) Green's function which corresponds to site i , and depends on the actual charge and magnetization density at this site i and, via the bath, at its neighboring sites in the stripe phase. In the presence of magnetic order the local Green's functions (3) are determined self-consistently together with local potentials $\Sigma_{i\sigma}^{\text{HF}}$. Thereby the total electron density,

$$\frac{1}{L} \sum_{i\sigma} n_{i\sigma} = n, \quad (9)$$

determines the chemical potential μ .

In order to solve the self-consistent problem posed by Eqs. (8), one has to find not only the HF (static) part of the self-energy, $\Sigma_{i\sigma}^{\text{HF}}$, given by electron densities, but also the dynamical part of the self-energy, $\Sigma_{i\sigma}^{\text{D}}(i\omega_\nu)$. The latter is the heart of the correlation problem in the DMFT.²⁷ Our earlier studies of the spectral properties of spiral phases in the doped Hubbard model⁴⁷ have shown that the accuracy of the dynamical part of the self-energy $\Sigma_{i\sigma}^{\text{D}}(i\omega_\nu)$ plays a central role for the nature of magnetic correlations in the ground state, and for its spectral properties. Therefore we have determined the site-dependent self-energy using an ED Lanczos algorithm³¹ for a single-impurity Anderson model (SIAM) at $T=0$, and verified that it is well suited to investigate the stripe phases. This nonperturbative approach allows for an accurate treatment of local spin and charge fluctuations, and is therefore exact in the limit of infinite dimension, $d \rightarrow \infty$.^{48,27} Thereby a lattice problem is mapped onto an effective SIAM, which is next solved self-consistently with the surrounding lattice. In the present case of a stripe phase, the unit cell of an AF domain is mapped onto a set of L different impurity models, with L self-consistency conditions, and the global constraint (9). Thus we considered an effective impurity model,

$$\begin{aligned} H_{\text{imp}}^{(i)} = & \sum_{\sigma} \epsilon_d c_{i\sigma}^{\dagger} c_{i\sigma} + U n_{i\uparrow} n_{i\downarrow} + \sum_{\sigma, k=1}^{n_s-1} \epsilon_{k\sigma}^{(i)} a_{k\sigma}^{\dagger} a_{k\sigma} \\ & + \sum_{\sigma, k=1}^{n_s-1} V_{k\sigma}^{(i)} (a_{k\sigma}^{\dagger} c_{i\sigma} + c_{i\sigma}^{\dagger} a_{k\sigma}), \end{aligned} \quad (10)$$

for each nonequivalent site $i = 1, \dots, L$. It includes $n_s - 1$ orbitals labeled by $k = 1, \dots, n_s - 1$, which couple to the impurity atom by real hybridization elements $V_{k\sigma}^{(i)}$, where the correlation problem is solved.

For the solution of the effective impurity model (10) with hybridization elements $V_{k\sigma}^{(i)}$, and orbital energies $\epsilon_{k\sigma}^{(i)}$ for

each nonequivalent site i in the stripe supercell, we employed the ED method of Caffarel and Krauth.³¹ The main advantage of this method is that it gives unbiased results for the self-energy and thus includes the leading local part of the dynamic processes which are responsible for the many-body behavior of interacting electrons. It is also very well suited to study the ground states of correlated systems, in contrast to QMC methods which can provide reliable information only at rather high temperatures, and therefore cannot be used to investigate the properties of the stripe phases. The same objection applies to the DMFT calculations which use an analytic form of the self-energy derived from spin fluctuations. In this case the spectral properties are strongly temperature dependent,^{29,47} and the stripes melt fast under increasing temperature.³⁰

The orbital energies for the conduction band $\epsilon_{k\sigma}^{(i)}$, and the corresponding hybridization elements $V_{k\sigma}^{(i)}$, are the effective parameters. In order to initialize the iteration it is sufficient to fix the noninteracting ($U=0$) impurity Green's function $\mathcal{G}_{i\sigma, n_s}(i\omega_\nu)$ at each atom i :

$$\mathcal{G}_{i\sigma, n_s}^{-1}(i\omega_\nu) = i\omega_\nu - \epsilon_d - \sum_{k=1}^{n_s-1} \frac{(V_{k\sigma}^{(i)})^2}{i\omega_\nu - \epsilon_{k\sigma}^{(i)}}. \quad (11)$$

The parameters $\{\epsilon_{k\sigma}^{(i)}, V_{k\sigma}^{(i)}\}$ are thereby fitted to reproduce the bath Green's function $\mathcal{G}_{i\sigma}(i\omega_\nu)$ by that found for the finite-orbital problem posed by the SIAM (10). The crucial step is the solution of the SIAM for $i = 1, \dots, L$ which serves to derive the impurity self-energies $\Sigma_{i\sigma}(i\omega_\nu)$ required for the next cycle. Therefore the numerical effort increases linearly with the size of the magnetic unit cell L in the stripe phase.

After solving the effective cluster problem using Lanczos algorithm, the local Green's function $G_{i\sigma}(i\omega_\nu)$ was determined. Self-consistency is implemented by extracting from Eq. (8) the new self-energy for $G_{ij\sigma}(\mathbf{k}, i\omega_\nu)$, and next employing Eq. (3) to start the next iteration. Finally, the parameters of the effective SIAM, $V_{k\sigma}^{(i)}$ and $\epsilon_{k\sigma}^{(i)}$, are obtained by fitting the bath problem represented by $\mathcal{G}_{i\sigma}(i\omega_\nu)$ to the cluster Green's function $\mathcal{G}_{i\sigma, n_s}(i\omega_\nu)$ on the imaginary energy axis. The best choice is obtained by minimizing the cost function,³¹

$$\chi_i^2 = \frac{1}{\nu_{\text{max}} + 1} \sum_{\nu=0}^{\nu_{\text{max}}} |\mathcal{G}_{i\sigma, n_s}^{-1}(i\omega_\nu) - \mathcal{G}_{i\sigma}^{-1}(i\omega_\nu)|, \quad (12)$$

for each impurity problem labeled by i .

Altogether, the present method might appear size dependent as it replaces a conduction band by a *finite* set of $n_s - 1$ orbitals. Of course, one could get an exact result for the dynamics in the impurity model only in the limit of $n_s \rightarrow \infty$. However, the convergence with the increasing cluster size is very fast, as established by Caffarel and Krauth for the metal-insulator transition in the Hubbard model,³¹ and thus they obtained reliable results already by solving the clusters with $n_s < 10$. We investigated the convergence of the Green's functions using different supercells with appropriate boundary conditions for a given type of stripe structure. In practice, we have solved the systems with $n_s = 6, 8, \text{ and } 10$, and veri-

fied that also in the present case of a stripe structure the convergence is exponentially fast. Therefore we present in Secs. III and IV the converged results obtained with $n_s=8$, and use them to discuss the physical properties of stable stripe phases in the 2D Hubbard model.

B. Physical quantities

After the self-consistent solutions for the local Green's functions (3) were obtained using different initial conditions, the ground state was determined by comparing the energy per site given by

$$E_0 = -\frac{i}{2\pi} \frac{1}{LN} \sum_{\mathbf{k}\sigma} \int_{-\infty}^0 d\omega e^{i\omega 0^+} \text{Tr}[\hat{h}(\mathbf{k}) \hat{G}_\sigma(\mathbf{k}, \omega)] - \frac{i}{4\pi} \frac{1}{L} \sum_{\sigma} \int_{-\infty}^0 d\omega e^{i\omega 0^+} \text{Tr}[\hat{\Sigma}_\sigma(\omega) \hat{G}_\sigma(\omega)], \quad (13)$$

where we considered a 2D lattice covered by N stripe supercells with L atoms each. For convenience, we have chosen the Fermi energy at $\mu=0$. This analysis led us to identifying the stable stripe phases in a broad regime of hole doping $0.03 < \delta < 0.20$, as discussed in Sec. III. The same approach allows us also to find the energies of the excited states with different types of stripe ordering, and the energy of the homogeneous paramagnetic phase.

The ground-state configuration is characterized by the electron density distribution $\{\langle n_{(l_x, l_y), \sigma} \rangle\}$, found from the local Green's function at each nonequivalent site $l=(l_x, l_y)$ in the stripe phase,

$$\langle n_{(l_x, l_y), \sigma} \rangle = -\frac{1}{\pi} \int_{-\infty}^0 d\omega \text{Im} G_{l\sigma}(\omega). \quad (14)$$

For a (01) stripe phase with vertical domain walls, one may label the atoms in the (magnetic) unit cell (which consists of a single row) by $l_x=1, \dots, L_x$. Therefore the charge distribution in this stripe phase is fully described by the average doped-hole density along the (10) direction, averaged over a single domain in a cluster with N_y atoms along the (01) direction,

$$n_h(l_x) = 1 - \frac{1}{N_y} \sum_{l_y=1}^{N_y} \langle n_{(l_x, l_y), \uparrow} + n_{(l_x, l_y), \downarrow} \rangle. \quad (15)$$

We considered the symmetry breaking with respect to the z th component of spin,

$$S_{(l_x, l_y)}^z = \frac{1}{2} [n_{(l_x, l_y), \uparrow} - n_{(l_x, l_y), \downarrow}], \quad (16)$$

which is related to the electron density operators in a standard way. The staggered magnetization density projected on the (10) direction in a vertical stripe phase,

$$S_\sigma(l_x) = \frac{1}{N_y} \sum_{l_y=1}^{N_y} (-1)^{l_x+l_y} \langle S_{(l_x, l_y)}^z \rangle, \quad (17)$$

is defined with a site-dependent factor $(-1)^{l_x+l_y}$ which compensates the modulation of the magnetization $\langle S_{(l_x, l_y)}^z \rangle$ within a single AF domain.

Charge response of the stripe phase is characterized by the static hole-hole correlation function,

$$C(\mathbf{k}) = \frac{1}{LN} \sum_{l_x, l_y} e^{-i(k_x l_x + k_y l_y)} \langle 1 - n_{(0,0)} \rangle \langle 1 - n_{(l_x, l_y)} \rangle, \quad (18)$$

where $\mathbf{k}=(k_x, k_y)$ is a vector from the first Brillouin zone (BZ). This function may be measured in elastic x-ray scattering. A similar spin-spin correlation function is defined by

$$S(\mathbf{k}) = \frac{1}{LN} \sum_{l_x, l_y} e^{-i(k_x l_x + k_y l_y)} \langle S_{(0,0)}^z \rangle \langle S_{(l_x, l_y)}^z \rangle, \quad (19)$$

which reproduces to leading order the measured two-particle correlation function in elastic neutron scattering — these experiments led to the discovery of the stripe ordering with half filled domain walls in the cuprates.²

Finally, the converged Green's functions were used to determine the spectral function in the stripe phases,

$$A(\mathbf{k}, \omega) = -\frac{1}{\pi} \frac{1}{LN} \text{Im} \sum_{mi, nj, \sigma} e^{-i\mathbf{k}(\mathbf{R}_{mi} - \mathbf{R}_{nj})} G_{mi, nj, \sigma}(\omega). \quad (20)$$

It is directly connected with the ARPES experiments and contains integrated information over different atoms of the magnetic supercell. By analyzing the spectral function we investigate in Sec. IV the momentum dependence of the quasiparticles near the Fermi energy and found a pseudogap which opens at the Fermi energy when the stripe order develops.

III. STRIPE ORDERING IN DIFFERENT DOPING REGIMES

A. Low doping regime: (11) stripes

We begin by reporting the stable ground states which were obtained as a result of extensive numerical calculations. We searched for self-consistent solutions with the lowest energy (13), starting from different initial conditions appropriate for various type of polaron and stripe ordering. We have chosen $U=12t$ for the numerical studies which gives the ratio of $J/t=1/3$ with $J=4t^2/U$, being a value representative for the cuprates.^{33,34} The Hubbard model with nearest-neighbor hopping only is appropriate for doped $\text{La}_{2-x}\text{Sr}_x\text{CuO}_4$ compounds, which exhibit the AF long-range order in a narrow range of $0 \leq \delta \leq 0.02$, followed by a spin-glass with a considerably lower transition temperature.^{11,49} The present DMFT calculations agree qualitatively with these experimental results, giving a robust AF state at $\delta=0$, and at small doping $\delta < 0.03$. Here the results support our earlier findings obtained using an analytic form of the self-energy which includes local spin fluctuations.²⁹ In fact, one might expect isolated polarons in this weakly doped regime, as found in the HF studies.^{1,13} Such local defects in the AF background are however rather extended in the present

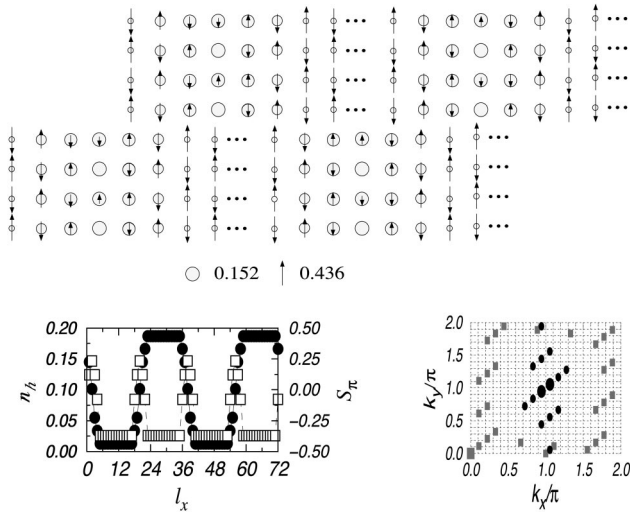


FIG. 1. Diagonal (11) stripe phase with a superimposed SDW as found at $\delta=1/20$ for $U=12t$. Top part shows doped hole (circles) and magnetization density (arrows) in the stripe 36×4 supercell. Lower part shows charge $n_h(l_x)$ [Eq. (15)] (empty squares) and magnetization $S_\pi(l_x)$ (filled circles) [Eq. (17)] density (left panel), and the charge $\mathcal{C}(\mathbf{k})$ [Eq. (18)] (squares) and spin $\mathcal{S}(\mathbf{k})$ [Eq. (19)] (circles) structure factors (right panel).

DMFT, and could not be stabilized within the considered clusters. Although we cannot make a definite conclusion, the numerical results suggest that the energy gains for local polarons would be very small indeed, and thus polarons would delocalize already at relatively low temperature.

We have found a *crossover* from a homogeneous AF phase *to stripe phases* which occur in a broad regime of low and intermediate doping $0.03 \leq \delta \leq 0.20$, and are remarkably stable when $\delta < 1/8$. In this doping regime polarons are already not expected as they were found to be unstable in several other calculations: HF,¹³ mean-field slave-boson approach,¹⁹ and variational studies performed within the local ansatz.²¹ Instead, we obtained a competition between three different types of stripe ordering, and the ground state changes twice: at $\delta \approx 0.05$ and at $\delta \approx 0.17$ doping.

The first stripe phase occurs at very low doping $0.03 < \delta \leq 0.05$ — it consists of *diagonal* (11) structures which are stabilized by a (weak) CDW superimposed with a SDW along the domain walls. This mechanism is to some extent analogous to that found at higher doping for vertical (01) stripes in HF.¹³ However, the diagonal stripes have a different nature, and were obtained here at a much lower doping. They may be seen as a precursor phase of (01) stripes, and demonstrate a generic tendency towards phase separation within a doped antiferromagnet (Mott insulator) into hole-poor and hole-rich regions.¹² As shown in Fig. 1, the stripes in this doping regime form extended structures, with their large unit cells involving a few atoms both along (10) and (01) directions. We have verified that the most stable structures for doping $\delta=1/20$ and $1/24$ have the magnetic unit cells with $L_y=4$ atoms along (01) direction, and $L_x=36$ and 40 atoms along (10) direction, which gives the total number of atoms within the unit cell $L=144$ and 160, respectively. The charge distribution is approximately the same along each

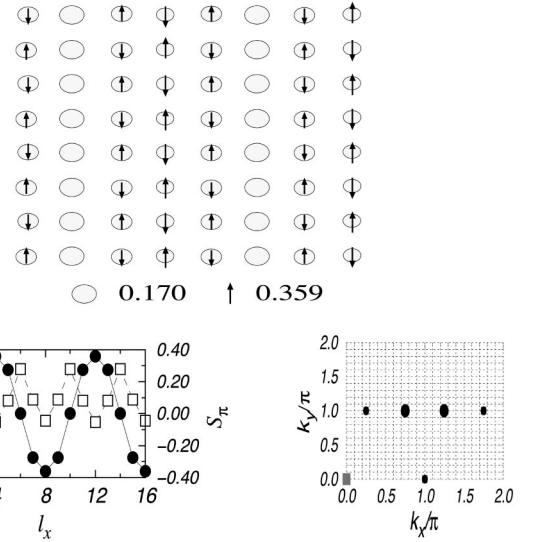


FIG. 2. Vertical site-centered (01) stripe phase for $\delta=0.125$ for $U=12t$ as obtained in the stripe 8×8 supercell. The meaning of different panels and symbols as in Fig. 1.

(10) row in a supercell, and involves a cluster of five atoms with enhanced hole density, which belong to an extended domain wall — there the increased hole density separates the AF domains, while the density within the domains remains almost unchanged with respect to the $n=1$ case.

The charge and magnetization distribution, given by Eqs. (15) and (17), respectively, found in the (11) stripe phase (Fig. 1) show a domain structure similar to that of (01) stripes at higher doping. The density of doped holes has a maximum at the central atom of a five-atom cluster, but it remains to some extent delocalized over the whole cluster. Note that the density distributions are symmetric with respect to the center of the domain wall, and this expected symmetry was obtained automatically as a result of the self-consistent solution of different SIAM problems coupled in a stripe supercell.

The (11) phase of Fig. 1 gives a quite involved charge response $\mathcal{C}(\mathbf{q})$ (18), with several weak maxima along the (11) direction which are likely to merge into a single broad peak in experiment, and result from the periodic charge distribution with large unit cells. The magnetic peak of the undoped AF phase at $\mathbf{Q}=(\pi, \pi)$ found in $\mathcal{S}(\mathbf{k})$ (19) splits off into two maxima at $\mathbf{Q}=[(1 \pm 2\eta_d)\pi, (1 \pm 2\eta_d)\pi]$, with $\eta_d \approx \delta/\sqrt{2}$. Such maxima were indeed observed in recent neutron experiments by Wakimoto *et al.*³² Remarkably, only two satellites could be resolved as in Fig. 1, indicating that the structural distortions present at low doping support a single easy direction for the formation of stripes.

B. Site-centered (01) stripes

In the intermediate regime of doping $0.05 < \delta < 0.17$, we have found *site-centered vertical stripes*, called below (01) phases, with an example shown in Fig. 2 for $\delta=1/8$. These structures have the nonmagnetic domain walls which separate the AF domains, and the magnetic unit cells contain between $L=16$ (at $\delta=1/16$) and $L=8$ (at $\delta \geq 1/8$) atoms. In

agreement with the experimental results in $\text{La}_{2-x-y}\text{Nd}_y\text{Sr}_x\text{CuO}_4$ (Ref. 2) and in $\text{La}_{2-x}\text{Sr}_x\text{CuO}_4$,²⁶ such states contain therefore 0.5 hole per charge unit cell (being half of the magnetic unit cell) as long as $\delta \leq 1/8$. We emphasize that the doped holes are much weaker localized at the domain walls than in the corresponding HF states, but still a distinct maximum of doped-hole density $n_h(l_x)$ is identified at the nonmagnetic domain walls, which is accompanied by a tail, extending within the magnetic domains, similar to the results of the slave-boson calculations¹⁹ and numerical DMRG, which also include explicitly electron correlation effects.²⁰ The average density at the nonmagnetic domain wall itself changes only weakly under increasing doping, with $n_i \approx 0.850$ and $n_i \approx 0.830$ at $\delta = 1/16$ and $1/8$, respectively, showing that the hole is somewhat more delocalized when the magnetic domains are smaller, and the doped holes start to overlap throughout the AF domains. This result corrects the previous more extreme views that the doped holes might be confined just to the domain walls, and each atom of the domain wall would then absorb 0.5 hole,^{2,13} while the AF domains would remain practically undoped.

Recently we pointed out²⁴ that the (01) stripe phases correspond to the observed periodicity of the vertical (01) stripe phase, with the shift of the neutron peak at $\mathbf{Q} = [(1 \pm 2\eta_v)\pi, \pi]$ given by $\eta_v = \delta$,²⁶ and thus we could identify half filled domain walls in the range of doping $\delta \leq 1/8$. We find it quite remarkable that the obtained (01) stripe phases are so robust, while, unlike in the HF states, where they are stabilized by the quadrupling of the period along the domain walls by either a SDW or CDW,¹³ there is no obvious mechanism in the DMFT which favors this filling. We come back to this question in Sec. IV A.

C. Melting of (01) stripes

The smallest charge unit cell for the (01) stripes contains four atoms: three of them belong to an AF domain, while the fourth atom belongs to the domain wall (see Fig. 2). Doping above $\delta = 1/8$ does not change the stripe unit cell anymore, but gradually weakens the stripe order. As a result, the doped holes tend to delocalize from the site-centered domain walls into the AF domains. First, the holes are doped almost uniformly with respect to the (more stable) phase at $\delta = 1/8$, with hole densities given by Eq. (15): $n_h(0) = 0.170$, $n_h(1) = 0.121$, and $n_h(2) = 0.088$ at the domain-wall atom ($l=0$), at its first ($l=1$) and at second ($l=2$) neighbor, respectively. For instance, the hole density increases almost uniformly by ~ 0.025 hole per atom to $n_h(0) = 0.192$, $n_h(1) = 0.145$, and $n_h(2) = 0.117$ when the doping increases to $\delta = 0.15$.

However, at higher doping the density of doped holes increases faster *within* the AF domains, and the amplitude of the CDW across the domains decreases (see Fig. 1 of Ref. 24). As a result, the site-centered stripes remain stable only until $\delta \approx 0.17$, while at higher doping stripe phases with *bond-centered domain walls* take over. An idealized stripe phase with such delocalized domain walls would consist of ladders of bond-centered domain walls with increased hole density and ferromagnetic order on the rungs, interchanging with the AF ladders with lower hole density and larger mag-

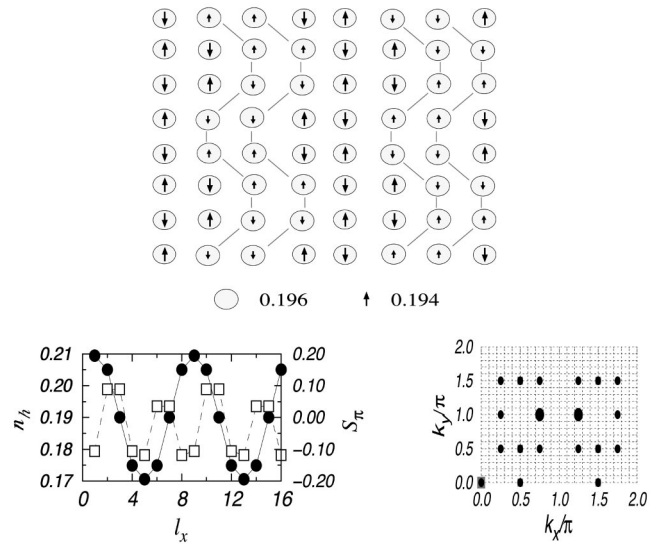


FIG. 3. Vertical bond-centered (01) stripe phase at $\delta = 0.1875$ for $U = 12t$ as obtained in the stripe 8×8 supercell. The meaning of different panels and symbols as in Fig. 1. Zigzag lines indicate the domain wall with small moments aligned on individual bonds.

netic moments, as obtained by White and Scalapino.²⁰ In contrast, we identified the stable bond-centered stripe phase being rather far from such idealized structures,²⁰ but involving *kinks and antikinks* which develop along the domain walls (see Fig. 3). They demonstrate that the optimal doping in domain walls is exceeded, and the holes cannot accommodate themselves on the vertical lines anymore but have to delocalize over more atoms, creating kinks and antikinks and increasing thereby the length of each domain wall. Another possibility could be that the domain walls tilt due to kinks ordered in one direction,⁵⁰ but the present studies indicate rather that a gradual delocalization into the bond-ordered domain walls takes place. It causes a change in the magnetic structure, and the doped holes start to make clusters of aligned spins. In such states hole propagation along the domain walls is still allowed. Note that the magnetization along the extended domain walls gives in this case a SDW with a periodicity of four atoms and thus one recovers a similar mechanism as found before in HF. Here it is present in the metallic phase, which helps to stabilize such extended domain walls in the range of doping where the stripe phases gradually melt.

We have found a small energy difference of typically less than $0.04t$ per doped hole between the site-centered and bond-centered domain walls, which are stable below/above $\delta = 0.17$, respectively. The bond-centered structures occur when the stripes at large doped-hole density fluctuate, and by this phenomenon release an additional kinetic energy.⁵¹ This energy gain could not be included in our calculations, and therefore one might expect that the bond-centered domain walls of Fig. 3 might be stable in an even somewhat broader regime of hole doping. Unfortunately, such structures give practically the same spin response as the site-centered stripes and are thus hardly distinguishable from them in neutron scattering and in ARPES spectroscopy.⁴²

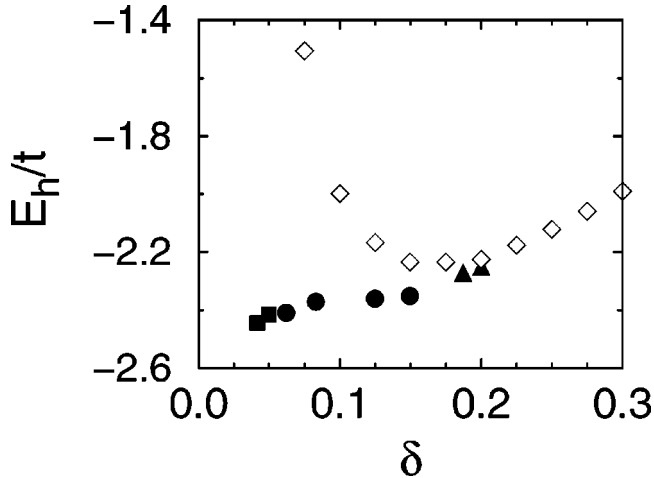


FIG. 4. Energy per doped hole E_h/t in the stable stripe phases (filled symbols) and in the doped paramagnet (empty diamonds) for $U=12t$. The stable stripe phases are found at $\delta < 0.20$: diagonal structures of Fig. 1 (squares), site-centered (01) stripe phases of Fig. 2 (circles), and bond-centered (01) stripe phases of Fig. 3 (triangles).

The stability of stripe phases at $\delta > 0$ depends on the tendency towards phase separation which may be investigated by the dependence of the energy normalized per one doped hole,¹³

$$E_h^S(\delta) = \frac{1}{\delta} [E_0(\delta) - E_{AF}(0)], \quad (21)$$

on doping δ . Here $E_0(\delta)$ is the ground-state energy (13) found for the most stable stripe phase at doping δ , and $E_{AF}(0)$ is the reference energy of an AF state in a Mott insulator at $\delta=0$, both found within the DMFT. As shown in Fig. 4, the energy $E_h^S(\delta)$ is a monotonically increasing function of doping, showing that the *stripe phases are stable against macroscopic phase separation*. We also note that it starts to increase somewhat faster with increasing δ when the doping exceeds $1/8$ which demonstrates a better stability of the (01) stripe phases at $\delta < 1/8$ and confirms that the doping $\delta=1/8$ may be considered as optimal for the (01) stripe phases.

In contrast, the *uniform* paramagnetic phase with the energy per hole given by

$$E_h^P(\delta) = \frac{1}{\delta} [E_P(\delta) - E_{AF}(0)], \quad (22)$$

decreases fast at low doping, and has a minimum at $\delta_m \approx 0.16$, with $E_h^P(\delta_m) \approx -2.23t$ ($-1.94t$) for $U=12t$ ($U=8t$). This indicates a generic tendency of the paramagnetic phase towards phase separation,⁵² as the lowest energy found at the minimum of $E_h^P(\delta)$ can be obtained just by separating the sample into the hole-poor (AF domain) and hole-rich (domain wall) regimes at any concentration $\delta \leq \delta_m$, following the Maxwell construction. It explains that the stripe phases are just a natural consequence of this instability, and the energy per hole found in them $E_h^S(\delta)$ is only somewhat lower than $E_h^P(\delta_m)$. Doping beyond δ_m soon destabilizes the stripes due to the domain-wall fluctuation as discussed

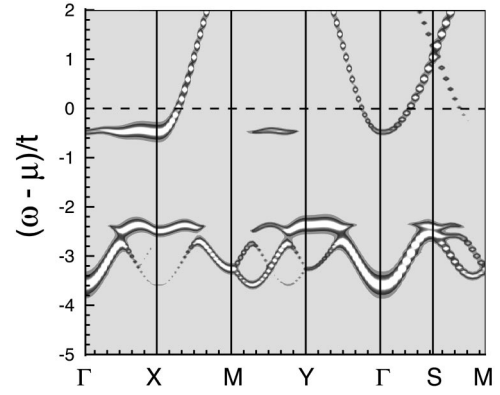


FIG. 5. Spectral function $A(\mathbf{k}, \omega)$ as obtained in the HF approximation for the (01) stripe phase with site-ordered nonmagnetic domain walls at $\delta=1/8$ for $U=12t$, along the main directions of the 2D BZ, with $\Gamma=(0,0)$, $X=(\pi,0)$, $Y=(0,\pi)$, $M=(\pi,\pi)$, and $S=(\pi/2,\pi/2)$. The largest spectral weight is found in white regions between the grey lines.

above, and the energies $E_h^S(\delta)$ and $E_h^P(\delta)$ merge above $\delta=0.20$. This estimate agrees well with the observed gradual disappearance of charge inhomogeneities in $\text{La}_{2-x}\text{Sr}_x\text{CuO}_4$ above the optimal doping.⁵³

IV. SPECTRAL PROPERTIES OF STRIPE PHASES

A. Metallic stripes in dynamical mean-field theory

In this section we want to concentrate first on two questions related to the stability of stripe ordering in doped anti-ferromagnets: (i) what is the mechanism which stands behind the stripe ordering; and (ii) how different is it from the well-known instabilities in HF,¹³ which are related to the extra periodicity of the SDW or CDW type? We will show that many-body correlations stabilize the stripe structures *without* this symmetry breaking, and thus the resulting states preserve to a large extent a 1D metallic behavior along the domain walls. To illustrate this point, we focus below on the spectral functions obtained in the (01) stripe phase for a representative value of $\delta=1/8$, using three different approximations: (i) the HF approximation, with the (static) local potentials (5) determined self-consistently, (ii) the so-called generalized HF (GHF) approximation,⁴⁷ where the charge fluctuations result in static screening of the local magnetic potentials, and (iii) the full self-consistent DMFT approach which includes both static screening and the dynamic correlations.

In order to address the above questions and to explain better the main features found in the spectral properties obtained for the stripe phases, we present first the spectral function (20) of tight-binding electrons moving in local magnetic potentials (5) corresponding to the magnetic domains of a (01) stripe phase. The self-consistently found stripe structure within the HF approximation is similar to that shown in Fig. 2, and the hole motion is coherent along the domain walls, as described by a 1D spin-degenerate band with dispersion

$$\varepsilon_{\mathbf{k}}^{1D} = -2t \cos k_y. \quad (23)$$

TABLE I. Values of local magnetization $m_i = |\langle S_i^z \rangle|$, and the on-site energy contributions V_i/t (26) as obtained in: HF, GHF, and DMFT for the (01) stripe phase at $\delta = 1/8$ (Fig. 2).

i	\bar{U}_i/U	m_i			V_i/t		
		HF	GHF	DMFT	HF	GHF	DMFT
0	0.273	0.0	0.0	0.0	0.0	0.0	0.0
1	0.934	0.456	0.393	0.275	2.50	1.73	0.86
2	0.997	0.475	0.468	0.359	2.71	2.62	1.54

It crosses the Fermi energy μ at $\mathbf{k} = (0, \pi/4)$, $(\pi, \pi/4)$, $(\pi/4, \pi/4)$, and equivalent points.

The result of a numerical calculation obtained for the doping of $\delta = 1/8$ is shown in Fig. 5. For this doping the magnetic unit cell contains again (as in the DMFT) eight atoms, and therefore one finds eight bands. The bands at low energy $-4t < \omega < -2t$ result from the propagation of a hole within the AF domains, and their top marks a large Mott-Hubbard gap which separates the lower Hubbard band (LHB) from the upper Hubbard band (UHB) (not shown) in a Mott insulator at $n = 1$. The doped hole moves independently from the other fermions and does not couple to the AF background in the HF approximation. Moving along the high-symmetry directions, parts of the bands have either only a rather weak spectral weight, or even vanish in the background. It happens for these parts of the BZ which lie outside of the AF folded zone, and the large weight is then found instead in the UHB, similar to a single hole doped to the Mott-Hubbard AF insulator.²⁹

Hole doping results in new dispersive states within the Mott-Hubbard gap:¹³ two (due to the folding of the BZ) mid-gap bands shown in Fig. 5. These quarter filled bands are crossed by the Fermi energy $\mu = 0$, and the system is metallic. An additional periodicity due to either a SDW or a CDW which might form along the domain walls would cause the gap opening at the points where the Fermi level is crossed by the 1D band (23) and thus lower the energy. However, such a gap would be small, and would not be sufficient to stabilize these structures globally.¹³ More importantly, such dispersive features at low energy are in striking contrast with the spectral densities measured in ARPES experiments for $\text{La}_{1.28}\text{Nd}_{0.6}\text{Sr}_{0.12}\text{CuO}_4$ (Ref. 39) and $\text{La}_{2-x}\text{Sr}_x\text{CuO}_4$,⁴⁵ where no spectral weight was found at the Fermi energy and close to it along the (11) direction, in particular at the $(\pi/4, \pi/4)$ point. The result of Fig. 5 shows, however, that a system with an empty 1D band (23) would be stable due to a large gap, being $\sim 1.8t$ for $U = 12t$, which separates this band from the remaining (filled) bands of the AF background. This case corresponds to the filled stripes observed in the nickelates, which are more classical and thus the HF picture is here closer to reality.^{14,15} It is straightforward to verify that such a phase is indeed more stable in the HF approximation as its energy per one doped hole (21) is lower.

We have shown in Sec. III A that electron correlations stabilize the half filled stripe phases for $\delta \leq 1/8$, and partly filled stripes for $1/8 < \delta < 0.20$. The reason of their stability becomes clear only when the spectral functions are investigated beyond the HF. We will distinguish now between the static and dynamic correlations which are both treated within

the DMFT, and consider first the generalized HF (GHF) approach in which the local Coulomb potentials (5) are screened by particle-particle scattering,^{54,55} and are thus replaced by effective site-dependent potentials,

$$\bar{U}_i = \frac{U}{1 + U\chi_i^{pp}(0)}, \quad (24)$$

with the renormalization obtained by a static particle-particle kernel ($k_B = 1$),

$$\chi_i^{pp}(0) = T \sum_{\nu} G_{i\uparrow}(i\omega_{\nu}) G_{i\downarrow}(-i\omega_{\nu}). \quad (25)$$

The calculations of the above vertex function $\chi_i^{pp}(0)$ were performed at finite but low temperature $T \approx 0.05t$, using the formalism developed in Ref. 55 for the magnetic states in the Hubbard model. As found before,^{47,55} the strongest screening of U occurs at nonmagnetic sites, while it gradually decreases with increasing local magnetization $m_i = \langle S_i^z \rangle$. The values of the screened potential are given in Table I. At the nonmagnetic domain-wall atoms one finds the screening of $\bar{U}_i/U = 0.273$ at $\delta = 1/8$ which is changing drastically the properties of electrons/holes from strong to weak correlations. As a result, the electrons *within* the domain walls behave differently and are still in the weakly correlated metallic regime, while the electrons within the AF domains experience an almost unscreened interaction, responsible for a large Mott-Hubbard gap in the electronic structure. Thus one encounters within the GHF an unprecedented separation into *almost uncorrelated* 1D electron gas coexisting with *strongly correlated* electrons responsible for the observed magnetic properties. The electron correlations cause also some decrease of the magnetization which is more pronounced at the atoms next to the domain walls (see Table I and Fig. 2).

The bands calculated within the GHF approximation are shown in Fig. 6. We have found that both the screening of local potentials \bar{U}_i (24), and a more uniform magnetization distribution than that determined in HF play an important role and modify the electronic structure. As a result of the local correlations, the gap between the 1D bands and the remaining AF bands closes, and the (empty) mid-gap bands hybridize strongly with the (occupied) AF bands in the LHB. Therefore some parts of the 1D band close to the Fermi energy lose their weight along the $\Gamma - Y$ and $\Gamma - S$ direction. On the contrary, the spectral weight along the $\Gamma - X$ direction which vanishes close to the Γ point, becomes *enhanced* at

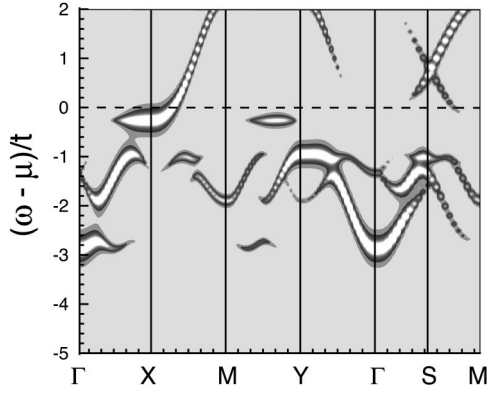


FIG. 6. Spectral function $A(\mathbf{k}, \omega)$ as obtained in the GHF approximation for the (01) stripe phase at $\delta=1/8$ for $U=12t$. The meaning of different symbols as in Fig. 5.

the X point and stays there below μ , as experimentally observed.^{39,45} The 1D band, still quite similar to the HF band, almost merges with an AF band below it, and in first approximation one might be tempted to consider the dispersive feature along the $\Gamma-X-M$ line as a single QP band of a large dispersion. This approximation predicts therefore that a band with a dispersion of $\sim 3t$ (only the part at $\omega < 0$), larger than that of the mid-gap state itself, might be observed in the ARPES experiments. This dispersion is of course far too large and not supported by the experimental observations. The polaronic band at the energy scale of $\sim J$ is absent in this approximation, as the local scattering processes of a hole on spin excitations are neglected within the GHF approach.

Dynamical correlations included in the DMFT modify both this ground state and the spectral properties. They are responsible for an even larger reduction of magnetization within the AF domains than that induced by the renormalized potentials (24) within the GHF. Altogether, the magnetic moments m_i are reduced by $\sim 40\%$ and $\sim 24\%$ with respect to the HF values at the first and second neighbors of the domain-wall atoms, respectively (Table I). Due to the ω dependence of the local self-energy which follows from the

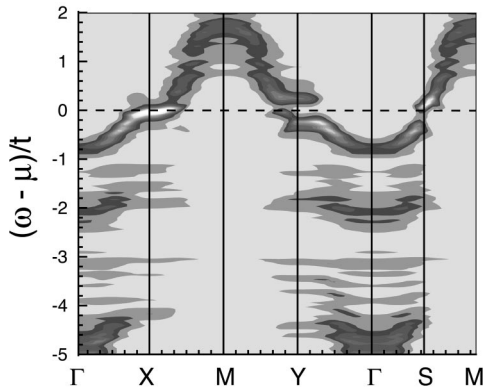


FIG. 7. Spectral function $A(\mathbf{k}, \omega)$ as obtained within the DMFT for the (01) stripe phase at $\delta=1/8$ for $U=12t$. The meaning of different symbols as in Fig. 5. The intensity of grey scale is proportional to the spectral weight.

DMFT, the change of the spectral functions from the GHF to the DMFT solution is even more dramatic than that between the HF and GHF results reported above. First of all, the spectral weight moves towards the Fermi energy for the \mathbf{k} points which belong to the AF BZ (Fig. 7). In this part of the BZ a large weight is found below the Fermi level μ — it consists of the *coherent QP band* with dispersion $\sim 2J$ at low energy (close to μ), and the *incoherent part* which extends in a range of $-6t < \omega < -t$. The latter has a rather characteristic weight distribution, with the large weight at $\omega \approx -5t$ near the Γ point, where the HF and GHF bands have their minima. This may be considered as a precursor feature of a free band with large dispersion of $8t$, which is finally obtained within the LHB in the limit of $n \rightarrow 0$ ($\delta \rightarrow 1$). The large spectral weight found at $\omega - \mu \approx -5t$ might be also understood as an antibonding state, resulting from the scattering processes at the correlated SIAM. It marks the low-energy edge of the LHB which has, together with the inverse photoemission (IPES) part which extends up to $\omega - \mu \approx 2t$, the width of $\sim 7t$, the same as found before for a single hole in the t - J model.⁵⁶

The *coherent* QP mode occurs as a consequence of the coupling of a moving hole to spin fluctuations at the impurity site, described within the DMFT by the SIAM (10). Such processes were absent in either HF or GHF static approaches. Here we find that the on-site spin dynamics is sufficient to generate a polaronic band, similar as it does for a single hole in an AF Mott insulator.²⁹ We emphasize that the momentum dependence of the QP pole follows in the DMFT approach entirely from the kinetic energy (6), which becomes strongly renormalized by the hole-magnon scattering down to a new energy scale $\sim J$. The QP dispersion extends over the energy range of $\sim 0.7t \approx 2J$, with $J/t = 4t/U = 1/3$. As expected, the polaronic band is distinct only within the AF BZ, where the noninteracting dispersion lies below the Fermi energy, $\varepsilon_{\mathbf{k}} = -2t(\cos k_x + \cos k_y) < \mu$. In general, the QP weight increases with the decreasing distance of $\varepsilon_{\mathbf{k}}$ from μ , as also found in the t - J model,⁵⁶ but the weight is somewhat differently distributed from that found for a single hole in the self-consistent Born approximation,⁵⁷ with a particularly large spectral weight near the $\mathbf{k} = (\pi, 0)$ point. The weakest QP is found near the Γ point, where more spectral weight is transferred to new incoherent structures which are generated at lower energies, while the QP spectral weight increases near the X, Y, and S points. The spectral weight is below μ in the remaining part of the BZ ($\varepsilon_{\mathbf{k}} > \mu$), where only shadow QP's are visible close to X, Y, and S points, and the incoherent spectral weight is very weak indeed, particularly at the M point. This shows that the electronic states at the Γ and at the M points are of completely different origin, and the matrix elements are of crucial importance when the spectra in the full BZ are constructed from those determined in the reduced AF BZ.

In the IPES part (at $\omega > \mu$), the spectrum changes in an even more dramatic way. The 1D band is washed out and instead a new dispersive feature develops which resembles the top of a 2D tight-binding band, with a similar \mathbf{k} dependence for the $\Gamma-X$ and $\Gamma-Y$ directions. By comparing the present result with the HF band structure it is clear that this

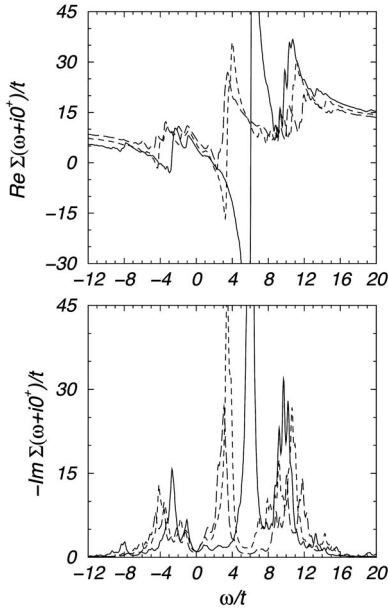


FIG. 8. Real (top) and imaginary (bottom) part of the local self-energy $\Sigma_{i\sigma}(\omega)$ as obtained within the DMFT for the site-centered (01) stripe of Fig. 2. Full, dashed, and long-dashed lines correspond to the atoms at the domain wall ($i=0$), and to the majority spin at the first ($i=1$) and second ($i=2$) neighbor of the domain wall, respectively.

feature has no relation to the QP states of the t - J model, but instead may be considered as a shadow of a free tight-binding dispersion in a strongly correlated stripe phase. This, in fact, demonstrates that the one-particle excitations in doped antiferromagnets have a very different nature below and above the Fermi energy.

The reasons for such strong changes of the spectral functions by dynamical correlations included within the DMFT become more transparent by looking at the self-energy. Near $\omega = \mu$ local self-energies $\Sigma_{i\sigma}(\omega)$ calculated for atoms $i=0, 1$, and 2 , respectively, exhibit the Fermi-liquid behavior with $\text{Im} \Sigma_{i\sigma}(\omega) \propto \omega^2$ (Fig. 8). We note, however, that our result is a Fermi liquid by construction, and the spin and charge order encountered in stripe phases, as well as the doping dependence of the chemical potential μ ,²⁴ indicate instead a non-Fermi-liquid regime. The separation into weakly and strongly correlated electrons is also observed in the self-energies, $\Sigma_{i\sigma}(\omega)$. While both atoms within the AF domains are similar, the dynamics at the domain walls is remarkably different due to the absence of the magnetic symmetry breaking term, and a strong screening of the local interaction \bar{U}_0 . This difference is particularly pronounced at $\omega \approx 2t$, where the QP states are practically absent within the AF domains, and would have there a very short lifetime. In contrast, the almost undamped excitations are possible at the domain walls themselves. This behavior demonstrates once again the quasi-1D metallic nature of the (01) stripe phases, with the hole hopping along the domain walls, being almost undamped by the scattering off the magnetic excitations. We also observed that the states in the UHB at $\omega \approx 10t$ have a rather low lifetime, in particular at the domain-wall atoms

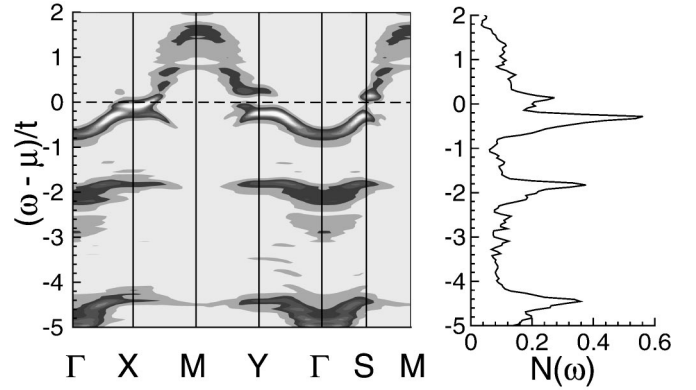


FIG. 9. Spectral function $A(\mathbf{k}, \omega)$ (left panel) and the density of states $N(\omega)$ (right panel) of the stripe phase at $\delta=1/12$ for $U=12t$. The meaning of different high-symmetry points is as in Fig. 5.

which may participate in such states only due to their hybridization with the neighboring magnetic atoms within the AF domains.

B. Doping dependence

Let us investigate now the changes of the spectral functions $A(\mathbf{k}, \omega)$ under increasing doping. We begin with the (01) stripe phase in the weakly doped regime at $\delta=1/12$ (Fig. 9). First of all, the characteristic spectral features in the LHB (the QP states at low energies $-0.7t < \omega < 0$, and the incoherent part at high energies $\omega < -t$) have again significant weight within the AF BZ, while the coherent mode in the IPES part ($\omega > 0$) is found outside the AF BZ, similar to the case of $\delta=1/8$. As in the $\delta=1/8$ case, the flat part of the QP band close to the X point is *below* the Fermi energy μ , and has an even larger spectral weight, as this channel of the hole dynamics is more important at low doping when the AF domains are still large and the hole-magnon coupling is more pronounced. The polaron band is more distinct at $\delta=1/12$ than at $\delta=1/8$, in agreement with the analysis of the wave function within the string picture.⁵⁸ At the same time, the weight in the low-energy IPES part is still low as there are only few empty sites, but the dispersive feature at $\omega > 0$ is already quite distinct.

We performed an extensive numerical simulation of spectral functions and found out that local magnetic energy contributions,

$$V_{i_x} \equiv \bar{U}_{i_x} \langle S_{i_x}^z \rangle^2 = \bar{U}_{i_x} m_{i_x}^2, \quad (26)$$

shown in Table I for $\delta=1/8$, play a crucial role not only for the stripe stability, but also determine the PES weight at μ for the $\mathbf{k}=(\pi/4, \pi/4)$ point. At the doping of $\delta=1/12$ the spin densities found in the DMFT give $V_1 \approx 0.99t$ and $V_2 \approx 2.07t$, where V_1 and V_2 are the above energy contributions (26) for the first and second neighbor of the domain-wall atoms, and lead to strongly suppressed PES weight at $(\pi/4, \pi/4)$. In contrast, increasing hole doping reduces these energy contributions. For instance, for $\delta=1/8$ doping one finds $V_1 \approx 0.86t$ and $V_2 \approx 1.54t$ (see Table I). Therefore the

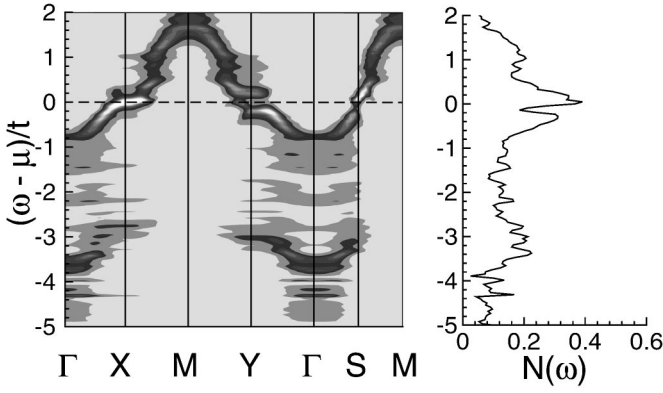


FIG. 10. Spectral function $A(\mathbf{k}, \omega)$ (left panel) and the density of states $N(\omega)$ (right panel) of the stripe phase at $\delta=0.15$ for $U=12t$. The meaning of different high-symmetry points is as in Fig. 5.

stripe order is here less stable than at $\delta=1/2$ and tends to disappear gradually above $\delta=1/8$, which is accompanied by a shift of the QP peak at the X point from the PES to the IPES part; at $\delta=1/8$ it is still almost precisely located at the Fermi energy μ .

With increasing doping δ the intensity is redistributed, as shown in Figs. 7 and 10. First of all, the weight of the dispersive state at $0 < \omega < 2t$ increases, as the spectral weight is transferred, both through the Fermi energy from the occupied to the unoccupied part of the LHB ($\omega < 0$), and from the UHB down to the IPES part of the LHB.⁵⁹ We emphasize that although a still simpler t - J model with the nearest-neighbor hopping element t which was recently successfully applied to describe several transport properties,⁶⁰ it misses part of the dynamics due to the three-site terms, and does not reproduce correctly the spectral weight transfers between the Hubbard subbands.⁵⁹ Therefore this simplification would not be appropriate for investigating the spectral properties at higher doping, particularly not in the regime of the IPES at low energy.

Also below the Fermi energy the spectral weight is modified and moves to higher energies, with the weak maximum of incoherent states found around $\omega \approx -3t$ at $\delta=0.15$. It replaces two maxima found before at $\omega \approx -2t$ and $\omega \approx -4.5t$ at $\delta=1/12$, while the incoherent spectral weight is smeared out over a broad energy range of $-6t < \omega < -t$. This shows that the AF order within the domains is gradually weakened by doping and the hole dynamics becomes more incoherent. This interpretation is also supported by the decreased spectral weight within the QP band close to $\omega=0$.

We observed only weak changes in the spectral functions at $\delta=0.1875$ doping, which shows that the actual charge and spin distribution plays only a secondary role and does not modify the spectral properties. They are mainly determined by the renormalized mid-gap band and by the polaronic band, in presence of the symmetry breaking between the (01) and (10) directions. If the value of U is decreased, the system becomes weakly correlated, the magnetic interaction $\propto J = 4t^2/U$ increases, and the length of the string of overturned spins, being proportional to $J^{-1/3}$,⁶¹ decreases, but the (01) stripe phase is still stable in a broad regime of doping. The

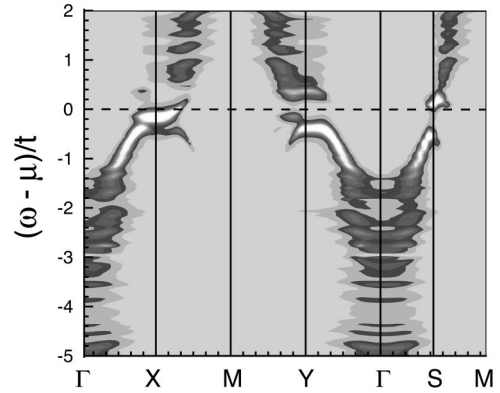


FIG. 11. Spectral function $A(\mathbf{k}, \omega)$ in the low-energy part as obtained for the (01) stripe phase at $\delta=1/12$ for $U=6t$. The meaning of different high-symmetry points is as in Fig. 5.

microscopic reasons of this behavior follow from the structure of the spin polaron, investigated in detail by Ramšak and Horsch.⁶² An example of the spectral function obtained when U is reduced by a factor of 2 down to $U=6t$ is illustrated in Fig. 11. The QP band is now found between $\omega = -1.7t$ and $-0.3t$, being again quite close to $2J \approx 1.33t$ and showing that the low-energy QP in the PES part is indeed of the polaronic origin. The spectral weight near the X point feature above μ extends also to higher energies than at $U=12t$, which proves that the dispersion in the IPES part is strongly renormalized by the hole-magnon scattering.

The evolution of low-energy features of the spectra in the range of $-2t < \omega < 0$ with increasing doping, shown in Figs. 7, 9, and 10, agrees very well with the recent results of the ARPES experiments on $\text{La}_{2-x}\text{Sr}_x\text{CuO}_4$.⁴⁵ First of all, in the weakly doped regime the top of the QP band is found at about -0.4 eV below the Fermi energy μ ,⁴⁵ and it has a similar intensity at the local maxima at the X and S points, with the maximum at the S point being somewhat closer to μ , as expected from the shape of the QP band at $\delta=0$.^{56,61} At $\delta=0.05$ a new feature appears at the X point close to μ , and its intensity increases rapidly with the doping up to $\delta \approx 0.12$. Simultaneously, the maximum of the spectral intensity moves towards μ , and is very close but still below the Fermi energy at $\delta=1/8$. This is precisely what we have also found in the present DMFT approach. Indeed, the QP peak is within our resolution precisely at the Fermi energy for $\delta=0.15$ (Fig. 10), while its maximum is somewhat broader at lower doping and lies about $0.15t$ below μ at $\delta=0.08$. This shift by $0.15t$ fits remarkably well to the shift of about 0.07 eV between $\delta=0.07$ and $\delta=0.15$, found in the experiment of Ino *et al.* (see Fig. 2 of Ref. 45). The QP maximum has almost no dispersion in a range of \mathbf{k} between $(3\pi/4, 0)$ and $(\pi, \pi/4)$ along the Γ -X-M line, as observed experimentally. As we explained in Sec. IV A, this behavior is characteristic for the metallic stripes.

The second characteristic feature observed by Ino *et al.* is the broad maximum at $\omega \sim -0.6$ eV below μ (see Fig. 4 of Ref. 45), with its intensity decreasing fast under increasing doping. We could also identify an intermediate energy feature at $\omega \approx -1.7t$ in our calculations, being particularly pro-

nounced at low doping both at the Y and S points, which next broadens and almost disappears around the optimal doping $\delta \approx 0.15$. We interpret this feature as the high-energy edge of the incoherent states in the LHB. However, we note that the experimental data give a large spectral weight around the X and S points, while in our calculations this feature is also strong around the Γ point. Of course, one has to realize that the present calculations do not include the matrix elements which are responsible for the final shape of the PES spectra, and thus we cannot expect a perfect agreement, in particular in the high-energy regime, where multiple scattering beyond sudden approximation is of importance.⁶³

C. Pseudogap in the metallic (01) stripes

The gross features of the spectra such as the Hubbard subbands separated by the large Mott-Hubbard gap appear due to on-site correlations induced by the large Coulomb interaction U . They arise independently of the type of magnetic order, and were found before for spiral phases and for paramagnetic systems at high temperatures.⁴⁷ By contrast, the low-energy QP's depend on the actual magnetic order. As a consequence of the stripe ordering, the spectra found along the $\Gamma-X-M$ path are not equivalent to those along the $\Gamma-Y-M$ one; at the Y point the polaronic band stays well below μ , and the spectral weight at $\omega = \mu$ almost vanishes. Also at the S point the QP band stays below $\omega = \mu$ and a pseudogap opens. On the contrary, the feature close to the X point changes into a flat QP state with a large intensity at the maximum, which is close to but still below $\omega = \mu$ for the present doping level of $\delta = 1/8$. It can be seen as a superposition of the flat 1D band for the holes propagating along the domain walls, and the spin polaronic band which stands for the hole propagation within the AF domains. As a result of strong hybridization between these two bands, we find that the coherent structure is almost flat also between $\mathbf{k} = (\pi, 0)$, and $\mathbf{k} = (\pi, \pi/4)$, where it finally crosses the Fermi level. This last feature agrees with the \mathbf{k} dependence of HF bands near the X point, but not near the other \mathbf{k} points. Altogether, the overall spectral weight distribution is quite different from the naive expectations based on the HF bands of Fig. 5, and does not agree with a partly filled spin polaron band which might be expected for the holes moving independently of each other within the AF domains.

A particularly interesting result is obtained along the $X-S-Y$ direction, with the QP peak which splits off at almost all the \mathbf{k} points, except in the vicinity of the X point into two structures below and above the Fermi energy μ , separated by a gap (Fig. 12). Also almost no spectral weight at μ is found along the $\Gamma-X$ and $\Gamma-Y$ directions, resulting thus in a distinct *pseudogap* in the density of states (Fig. 13). It opens between the polaron QP band and the mid-gap band which is so characteristic of the metallic stripe phase.⁴⁰

The experimental evidence of a pseudogap, which has been observed in the normal phase of all HTS's, comes in first place from the ARPES experiments.^{39,45} Other experimental techniques which do not provide information about single electronic states, but involve a transition from an initial occupied to a final empty state, include transport proper-

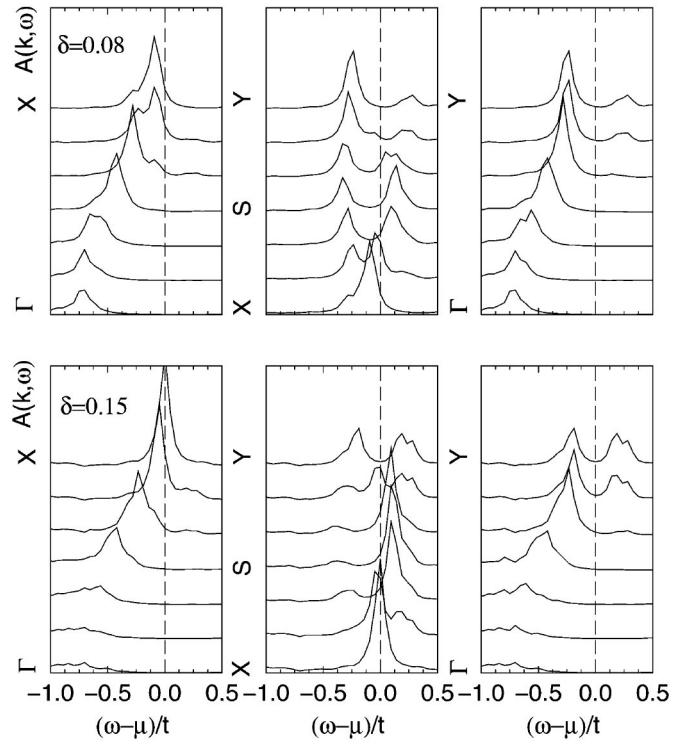


FIG. 12. Spectral functions $A(\mathbf{k}, \omega)$ along the main directions of the 2D BZ as obtained in the stripe phases at doping: $\delta = 1/12$ (upper panels) and $\delta = 0.15$ (lower panels). The meaning of different high-symmetry points is as in Fig. 5.

ties, specific-heat measurements, magnetic neutron scattering and nuclear magnetic resonance, also indicate that a (pseudo)gap opens around the Fermi energy in the superconducting cuprates.⁶⁴ Our calculations show explicitly that the gap at the Fermi level follows from static stripes in

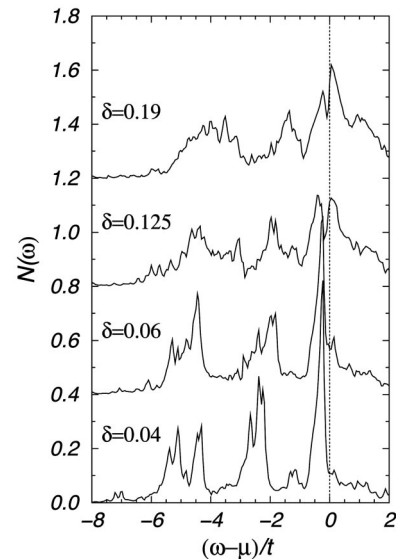


FIG. 13. Evolution of the density of states $N(\omega)$ as obtained at doping $\delta = 0.04, 0.06, 0.125,$ and 0.19 , in the stable stripe phases for $U = 12t$. The pseudogap visible at the Fermi energy $\omega = \mu$ separates the PES from the IPES part.

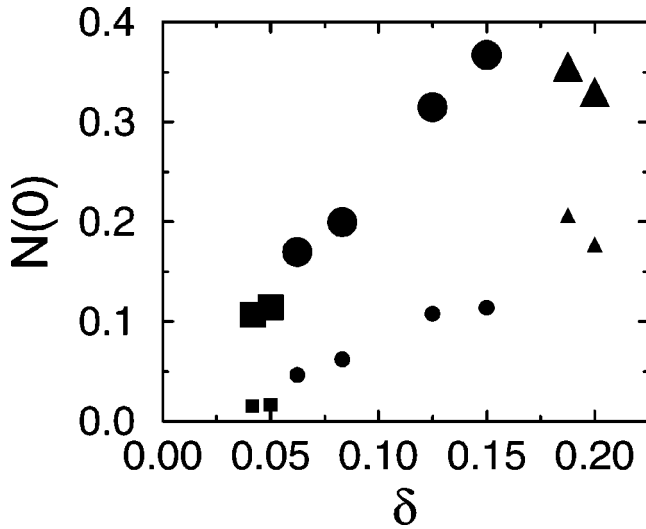


FIG. 14. Density of states $N(0)$ at the Fermi energy as obtained in different stripe phases for $U=12t$: diagonal (squares), site-center vertical (circles) and bond-center vertical (triangles). Large (small) symbols correspond to the total density of states and to its part due to domain-wall atom, respectively, both normalized to the stripe supercell.

$\text{La}_{2-x}\text{Sr}_x\text{CuO}_4$ compounds and may be considered as an *electron correlation effect* in the electronic structure. It opens in the density of states $N(\omega)$ around $\omega=0$ with the onset of stripe phases, and persists in the whole regime of doping $0.03 < \delta < 0.20$, where the stripes are stable, but gradually fills up with the spectral weight when the stripes melt (Fig. 13). The large peak in $N(\omega)$ found for $\omega - \mu > -0.7t$ in the PES part, which originates from the QP polaron band, is well separated from the domain-wall band in the IPES part. The features at low $\omega < -t$ are more and more smeared out with increasing doping, showing that the scattering within the LHB becomes gradually more incoherent.

As the pseudogap opens right at the Fermi energy, the density of states $N(0)$ at $\omega=0$ is rather low. In fact, the large spectral weight close to μ at and near the X point falls within the pseudogap in the range of doping $0.05 \leq \delta \leq 0.15$, but it has low weight in the integrated spectral density. We have found that it increases almost linearly when the doping δ increases in the range of $0.04 < \delta < 0.15$ (Fig. 14), and next flattens out and even slightly decreases when $\delta > 0.17$, where the stripes melt and the spectral weight at the X point is already above the Fermi energy. The dominating contribution to $N(0)$ comes from the QP structures near the X point, and shows a similar increase to that obtained by Ino *et al.* for the integrated spectral weight at the X point.⁴⁵ The results presented in Fig. 14 indicate that a maximum observed in the γ coefficient of the low-temperature specific heat,⁶⁵ $C_V \sim \gamma T$, proportional also to the effective mass m^* , develops as a natural consequence of the crossover from the stripe phases, stable in the normal state of La-based superconductors, to the Fermi-liquid regime above the optimal doping.

It is remarkable that the domain-wall atoms contribute about one third of $N(0)$ in the (01) stripe phases, almost independently of the size of the charge unit cell. This dem-

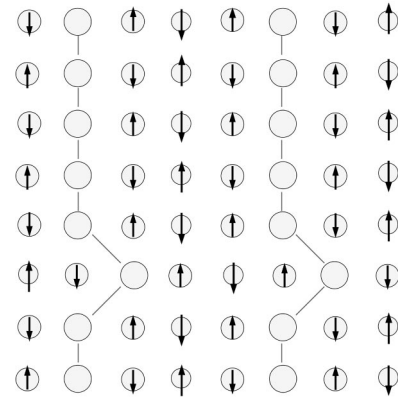


FIG. 15. Doped-hole and magnetization density as obtained in the vertical (01) stripe phase with a single kink along the domain wall within an 8×8 supercell, for $\delta=1/8$, $t' = -0.33t$, $t''=0.17t$, and $U=12t$.

onstrates that the low-energy spectral weight, and the thermodynamic properties at low temperatures in the normal phase, are to a large extent driven by the 1D metallic behavior along the stripes in $\text{La}_{2-x}\text{Sr}_x\text{CuO}_4$. Only in the diagonal structures at $\delta \leq 0.05$ the contribution of the domain-wall atoms is less significant, as the walls are then more delocalized (see Fig. 1), and cannot be represented by contributions from individual atoms in the center of the walls.

V. STRIPES IN THE MODEL WITH EXTENDED HOPPING

One of the outstanding questions is why the stripe phases are not observed in the Y- and Bi-based HTS's. We argue that the principal reason why these phases are unstable are higher values of the second and third neighbor hopping than in $\text{La}_{2-x}\text{Sr}_x\text{CuO}_4$ compounds, and these hopping processes destabilize the (01) stripe phases described in Sec. IV. One expects that for more extended hopping quantum fluctuations should give another energy contribution which would destabilize the (01) stripe structures in the higher doping regime. Although we could not obtain such energy contributions which follow from the fluctuations of the stripe structures, we investigated the effect of a single kink along the (01) domain wall in an 8×8 cluster, which stands for the magnetic stripe supercell in this case (Fig. 15), using the DMFT. For the doping of $\delta=1/8$, which is optimal for the (01) stripe phase with the magnetic unit cell consisting of eight atoms, the kink costs energy at $t'=0$, as it disturbs the hopping of holes along the vertical domain walls (Table II). Small t' , as found in $\text{La}_{2-x}\text{Sr}_x\text{CuO}_4$, has almost no effect on the energy of the (01) stripe phase — in fact the energy cost of forming a kink even slightly *increases* up to $t' = -0.1t$, and we believe that this follows from the proximity of the Fermi energy to the van Hove singularity in the noninteracting band structure, which moves to lower energies at finite t' .⁵⁵ This agrees with the softening of the stripe tension which was observed recently within the effective band model.⁶⁶ However, at $t'/t < -0.1$ the opposite trend was observed, and the energy to form a kink decreases fast with increasing $|t'|$, and finally the wall with a kink becomes favored at $t' \lesssim -0.3t$.

TABLE II. Energies per hole (21) obtained using an 8×8 stripe supercell in the (01) stripe phase: without ($E_{(01)}/t$), and with (E_{kink}/t) a single kink along each domain wall (shown in Fig. 15), and the energy difference $\Delta E/t = [E_{\text{kink}} - E_{(01)}]/t$, for different values of t'/t . Parameters: $\delta = 1/8$, $t'' = -0.5t'$, and $U = 12t$.

t'/t	$E_{(01)}/t$	E_{kink}/t	$\Delta E/t (\times 10^{-3})$
0.0	-2.3599	-2.3499	10.0
-0.05	-2.3444	-2.3340	10.4
-0.10	-2.3788	-2.3664	12.4
-0.15	-2.4190	-2.4132	5.8
-0.20	-2.4738	-2.4684	5.4
-0.25	-2.5462	-2.5418	4.4
-0.30	-2.6218	-2.6220	-0.2
-0.35	-2.7300	-2.7468	-16.8

Thus the regime of parameters encountered in the HTS with $T_c \approx 100$ K is characterized by *transverse kink fluctuations* in the normal state. We believe that these strong fluctuations along individual domain walls are responsible for the apparent difficulty to observe the static stripes in these compounds.

If the hopping becomes more extended, and the effective Hubbard model contains also sizable second ($t' = -0.33t$) and third ($t'' = 0.17t$) neighbor hopping,³³ several changes in the spectral functions occur. Here we present the data obtained for (01) stripe phases which are believed to be representative also for fluctuating stripe phases. Although the spin-polaron band appears again below the Fermi energy $\mu = 0$, it is modified in a similar way to that known from the earlier studies of a single-hole dispersion in the t - t' - J model (Fig. 16).⁶⁷ Due to the diagonal hopping element t' the dispersion along the Γ - X and Γ - Y directions decreases, while it remains almost unchanged along the diagonal Γ - S direction, giving again a QP bandwidth close to $2J$. This induces rather strong changes in the overall distribution of the spectral weight at low energies. At low doping $\delta = 1/12$ the polaron band is found well below μ at the X point, and the QP state at this point is rather broad. However, this band

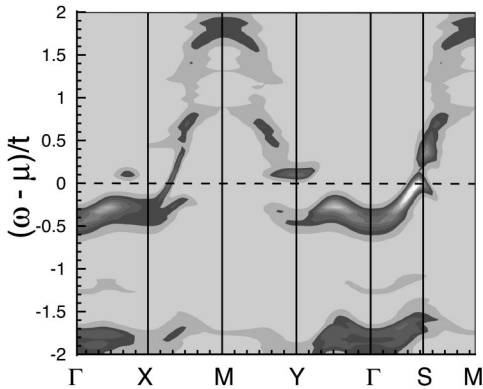


FIG. 16. Spectral function $A(\mathbf{k}, \omega)$ of the (01) stripe phase at $\delta = 1/12$ for $U = 12t$, and with the extended hopping: $t' = -0.33t$ and $t'' = 0.17t$. The meaning of different high-symmetry points is as in Fig. 5.

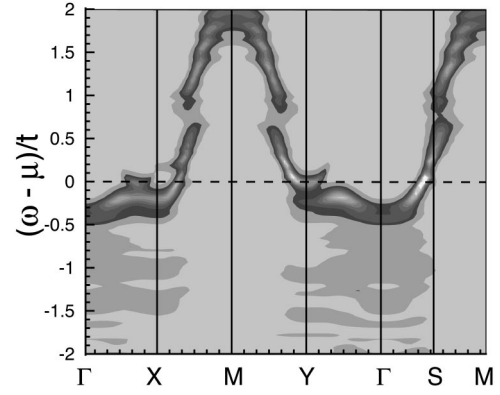


FIG. 17. Spectral function $A(\mathbf{k}, \omega)$ of the (01) stripe phase at $\delta = 0.15$. Parameters are the same as in Fig. 16.

hybridizes again with the mid-gap band induced by the non-magnetic domain-wall atoms just above $\mu = 0$, and thus these two features happen to merge at the X point, a dispersive state continues along the the X - M line, and crosses μ at $\approx (\pi, \pi/4)$, quite close indeed to the intersection expected for the corresponding band structure in the HF approximation. This strong hybridization near the X point is responsible for the metallic behavior of the system in the vertical (01) stripe phase.

Due to the increased diagonal (11) hopping, the gap which opened before (at $t' = 0$) at the S point (Figs. 2, 9, and 10), closes, and the polaron band continues smoothly through the Fermi energy. This band has now the largest dispersion along the Γ - S direction, similar to the one-hole case,⁶⁷ and the hybridization with the mid-gap band enhances the coherent spectral weight of the QP state close to the S point. On the contrary, the polaron band does not hybridize with the mid-gap state at the Y point, where an even larger gap than in the $t' = 0$ case opens at μ . Nevertheless, when the spectral density is integrated over the \mathbf{k} points, the large spectral weight found around $\omega \approx \mu$ close to the S and equivalent points dominates at low energies in the present spectra, and is responsible for the closing of pseudogap. It agrees very well with the sharp peak observed at μ , both for the underdoped and overdoped $\text{Bi}_2\text{Sr}_2\text{Cu}_2\text{O}_{8+x}$.⁶⁸

With increasing doping the dispersive state above μ becomes more distinct, and starts to hybridize with the polaron band even at the Y point, where no spectral weight was found before (Fig. 17). This change occurs as the hole penetrates now easier *across* the domain walls due to a more extended hopping. In fact, the mid-gap state close to the Y point almost merges with the maximum of the QP band along the Γ - Y line, showing that two different physical processes are responsible for the low-energy spectral properties at this point. The pseudogap does not open also at the higher doping due to a large spectral weight along the (11) direction, what is consistent with our expectations confirmed by the experiment that the (01) stripes are unstable for the present values of the hopping elements: $t' = -0.33t$ and $t'' = 0.17t$.

VI. SUMMARY AND CONCLUSIONS

We have presented a generalization of the DMFT approach to stripe phases in the Hubbard model at $T = 0$. This

approach, combined with the ED method to determine the local self-energies, allows us to obtain the evolution of stripe phases with increasing doping which agrees remarkably well with the experimental observations in $\text{La}_{2-x}\text{Sr}_x\text{CuO}_4$ materials. The present study demonstrates the importance of *local correlations* which play a crucial role in stabilizing the stripe phases having the same periodicity and regions of stability as observed experimentally.^{2,26,49} We have verified that inaccurate forms of the self-energy lead always to higher energies per doped hole, and the presented here stripe ordering is destabilized.

While the tendency towards charge and spin ordering in a form of stripe phases may be understood as a compromise which follows from optimizing the kinetic energy $\propto t$ and the magnetic energy $\propto J$ at the same time, the detailed mechanism of this instability is still under investigation. First of all, the HF studies have clarified that the largest kinetic energy gains are obtained due to the hopping elements t_\perp *perpendicular* to the (01) stripes by the solitonic mechanism,^{13,17} while the elements t_\parallel *parallel* to the (01) stripes are less important for their stability. Therefore it might be expected that the stripe ordering will always tune the direction of the domain walls along a weaker hopping in the anisotropic model, realizing the condition $t_\perp > t_\parallel$, and indeed this trend was confirmed by recent numerical simulations within the t - J model.⁶⁹ In contrast, there are more parallel AF bonds than perpendicular ones to the direction of the (nonmagnetic) domain walls, and therefore an increasing superexchange *parallel* to the domain walls J_\parallel will have a stabilizing effect on the (01) stripes. We expect that these tendencies are general and occur in the (11) stripes as well, with the second neighbor hopping t' across the (11) stripes and exchange elements J' along them playing a similar role for the stability of such phases.

The main conclusions of the present study concern the spectral properties of the stripe phases. The spectral functions $A(\mathbf{k}, \omega)$ obtained within the DMFT for the stripe phases, analyzed here for a realistic value of the local Coulomb interaction $U = 12t$, consist of the LHB and the UHB, separated by the Mott-Hubbard gap $\propto U$, and these dominating features manifest the strong correlations and are thus almost independent of the magnetic order. In contrast, the spectral weight distribution near the Fermi energy μ is very sensitive to the type of magnetic order and allowed us to identify the spectroscopic consequences of the stripe phases. We could derive systematic changes of $A(\mathbf{k}, \omega)$ within the LHB when the system is doped and the ground state changes from the AF insulator at $\delta = 0$ to stripe phases at $\delta > 0$. The doping modifies strongly the LHB and leads to three main features at $\omega < \mu$: (i) incoherent part at low energy $\omega - \mu \sim -4.8t$, (ii) folded bands due to stripe supercell at intermediate energy $\omega - \mu \sim -2.0t$, and (iii) low-energy QP states of the spin-polaron band. These distinct features of the LHB agree very well with recent QMC calculations.⁷⁰ We emphasize that the low-energy polaron band represents a coherent part of the LHB, and appears as expected within the Mott-Hubbard gap in a strongly correlated system. At the same time, a new dispersive feature above the Fermi energy develops gradually to a band. It originates from the partly filled

mid-gap band found in the HF approximation for the stripe superstructure, but is strongly renormalized by spin fluctuations.

The changes of the polaron band under increasing doping demonstrate that the rigid band approximation does not apply to the electronic structure of stripe phases, and the QP dispersions determined for a single hole moving in an AF background^{56,61} can only be used to interpret the experimental data at very low doping $\delta \lesssim 0.03$. The strong renormalization of the QP band with the mid-gap band plays a prominent role in breaking the symmetry between the X and Y points in (01) [or equivalent (10)] stripe phases. The noninteracting mid-gap band lies well above the Fermi energy at the Y point, and thus the polaron band is here only weakly influenced, and a gap for charge excitations opens at the Fermi energy. Similar weight distribution, with a gap for charge excitations was obtained at the $S = (\pi/2, \pi/2)$ point, and the noninteracting band crossing μ at $\mathbf{k} = (\pi/2, \pi/2)$ was eliminated. On the contrary, the hybridization between the polaron band and the mid-gap band is very strong close to the $X = (\pi, 0)$ point, resulting in a flat QP state which is almost pinned to μ . It stays *below* μ at doping $\delta < 1/8$, and next it approaches the Fermi energy, passes it, and finally moves to higher energies *above* μ when the (01) stripe phase gets overdoped. This explains the physical origin of the flat QP state observed near the X point in $\text{La}_{2-x}\text{Sr}_x\text{CuO}_4$.⁴⁵

Our conclusions concerning the \mathbf{k} dependence of the spectra are similar to those obtained recently by simulating the stripe phases either in an analytic approach of Wróbel and Eder,⁴¹ and in numerical studies using either a cluster perturbation theory,⁴² or the Monte Carlo method.⁴⁴ All these studies have shown in a very transparent way that electron correlations present in stripe (01) phases are responsible for the strong hybridization between the spin polaron band and the mid-gap stripe band which leads to the flat QP state near the X point, and for a gap which opens at the S point. It was pointed out recently that the above features observed in PES could be simulated in the t - J model only after including anisotropic spin-spin interactions on the domain walls.⁴³ Such terms replace in their phenomenological approach local correlations which were shown by us to give different screening of \bar{U}_i (24), depending on the atom position in the stripe supercell.

As a second important conclusion, stripe phases are *metallic*, and we could not confirm the *insulating* stripes discovered in the HF studies.^{1,13} Instead we show that the physical processes of dynamical nature which occur at low energies play a decisive role for the metallicity of stripe phases. Precisely for this reason the coupling between a hole and spin excitations cannot be neglected, if the spectral properties are investigated. Our study demonstrates that the metallic behavior occurs notably due to quantum fluctuations which strongly screen the Coulomb elements U_i on the domain walls, which coexist with much larger magnetic potentials within the AF domain walls. As a result, the spectra show simultaneously features characteristic to both *strongly* and *weakly* correlated systems. On one hand, the electrons move easier *along* the (01) vertical domain walls where they do not experience the alternating potential, while this motion is hin-

dered by the magnetic order within the AF domains. On the other hand, the electron motion across the domain walls is disturbed due to the potential barrier, but becomes possible as tunneling processes when the electron is dressed by spin fluctuations. Therefore the metallic behavior follows from the tunneling which is enhanced when the (01) stripe phase is overdoped, i.e., in the regime of $\delta > 1/8$. Similar conclusions were deduced recently by Moreo *et al.*⁴⁴ for the stripe phases in the spin-fermion model.

The present study shows that the pseudogap observed in the cuprates⁴⁵ follows in an intricate way from the stripe ordering. Gaps found for the charge excitations close to μ for all the points within the AF BZ except in the vicinity of the X point reproduce a pseudogap which is pinned to μ . Therefore, in spite of their metallicity, *the stripe phases show a non-Fermi-liquid behavior* in a broad regime of doping, in particular for $\delta < 1/8$. This is confirmed by the chemical potential μ which shifts downwards with hole doping,²⁴ $\Delta\mu \propto -\delta^2$, in agreement with the experimental data of Ino *et al.*,³⁶ and with the results of Monte Carlo simulations of the 2D Hubbard model.⁷³ We emphasize that the pseudogap is a very characteristic feature of the systems which exhibit phase separation, as has been experimentally observed also in the colossal magnetoresistance manganites.^{71,72}

It has been established experimentally that the stripe phases and a pseudogap exist only below a certain characteristic temperature T^* of the order of $\sim 0.05t$.⁶⁴ This temperature is in the range of the excitations in stripe phases,²⁴ and we also found a similar energy difference between the site-ordered and bond-ordered stripe phases. This explains why the spectral properties at high temperatures $T > T^*$ are so different, and are dominated by broad dispersive features which originate from local processes due to on-site electron correlations.^{47,74} In contrast, the quantum coherence which leads to the observed distinct QP peak at the $X = (\pi, 0)$ point, and the charge gap between well defined QP states at the $S = (\pi/2, \pi/2)$ point, can develop only at sufficiently low temperatures $T < T^*$, where the stripe phases are stable. These features were both obtained within our calculations, showing that the local correlations described by the Hubbard model at large $U \approx 12t$ are sufficient to explain the experimental data for $\text{La}_{2-x}\text{Sr}_x\text{CuO}_4$.⁴⁵

Finally, the present study allows to understand the physical reasons behind the observed differences between the ARPES spectra of $\text{Bi}_2\text{Sr}_2\text{CaCu}_2\text{O}_{8+y}$,^{37,38} and $\text{La}_{2-x}\text{Sr}_x\text{CuO}_4$ systems.⁴⁵ The generic picture obtained using

the Hubbard model with nearest-neighbor hopping is adequate only for the $\text{La}_{2-x}\text{Sr}_x\text{CuO}_4$ compounds, where the extended hopping plays no role. We have shown that the spectral properties are strongly modified when the hopping to second (t') and third (t'') neighbors is sizable, as in other HTS's. It moves the QP peak close to the S point, and closes the gap at the Fermi energy. We believe that the extended hopping terms $\propto t'$ and $\propto t''$ have far reaching consequences near the optimal doping than just the presented changes of the QP dispersion at low energies, influencing *inter alia* the actual value of transition temperature T_c ,⁷⁵ and they will be addressed in more detail by future studies. In their presence the stripe phases become softer, and kink fluctuations are more easily generated. They are likely to destabilize the stripes at lower temperatures, and thus explain why static stripes could not be observed in other than $\text{La}_{2-x}\text{Sr}_x\text{CuO}_4$ systems until now.^{2,35} However, they could also lead to other forms of short-range magnetic order which might be responsible for a pseudogap in Y- and Bi-based cuprates. It would also be interesting to investigate the stripe phases in electron doped HTS's,⁷⁶ once their effective parameters were derived from the charge-transfer model. Another challenging problem for future studies is the relation of the stripe order to the electron fractionalization in the cuprates.⁷⁷

Summarizing, we have shown that the local correlations captured within the DMFT lead to stable stripe phases in a broad range of hole doping, and reproduces the experimental results. These correlations are responsible for the characteristic momentum dependence of the spectral properties and provide a microscopic explanation of such prominent features measured in the ARPES of $\text{La}_{2-x}\text{Sr}_x\text{CuO}_4$ at low and intermediate doping as the flat QP state near the X point and the gap at the S point, being signatures of the (01) stripe ordering. In contrast, these stripe phases are destabilized by kink fluctuations in Y- and Bi-based HTS's, and the extended hopping leads there to the enhanced spectral weight along the (11) direction and to the distinct QP states close to μ at the S point, also observed in the ARPES experiments.

ACKNOWLEDGMENTS

We thank O. K. Andersen, A. Greco, B. Keimer, B. Normand, E. Pavarini, S. Sachdev, and J. Zaanen for stimulating discussions. A.M.O. acknowledges the support by the Committee of Scientific Research (KBN) of Poland, Project No. 5 P03B 055 20.

¹J. Zaanen and O. Gunnarsson, Phys. Rev. B **40**, 7391 (1989); D. Poilblanc and T. M. Rice, *ibid.* **39**, 9749 (1989); M. Kato, K. Machida, H. Nakanishi, and M. Fujita, J. Phys. Soc. Jpn. **59**, 1047 (1990).

²J. M. Tranquada, B. J. Sternlieb, J. D. Axe, Y. Nakamura, and S. Uchida, Nature (London) **375**, 561 (1995); J. M. Tranquada, J. D. Axe, N. Ichikawa, Y. Nakamura, S. Uchida, and B. Nachumi, Phys. Rev. B **54**, 7489 (1996).

³C. Nayak and F. Wilczek, Phys. Rev. Lett. **78**, 2465 (1997).

⁴J. Zaanen, J. Phys. Chem. Solids **59**, 1769 (1998).

⁵T. Mizokawa and A. Fujimori, Phys. Rev. Lett. **80**, 1320 (1998).

⁶M. Imada, A. Fujimori, and Y. Tokura, Rev. Mod. Phys. **70**, 1039 (1998).

⁷T. Tohyama, S. Nagai, Y. Shibata, and S. Maekawa, Phys. Rev. Lett. **82**, 4910 (1999).

⁸M. Vojta and S. Sachdev, Phys. Rev. Lett. **83**, 3916 (1999).

⁹S. Chakravarty, R. B. Laughlin, D. K. Morr, and C. Nayak, Phys. Rev. B **63**, 094503 (2001).

- ¹⁰M. A. Kastner, R. J. Birgeneau, G. Shirane, and Y. Endoh, *Rev. Mod. Phys.* **70**, 897 (1998).
- ¹¹C. Niedermayer, C. Bernhard, T. Blasius, A. Golnik, A. Moodenbaugh, and J. I. Budnick, *Phys. Rev. Lett.* **80**, 3843 (1998).
- ¹²V. J. Emery and S. A. Kivelson, *Physica C* **209**, 597 (1993).
- ¹³J. Zaanen and A. M. Oleś, *Ann. Phys. (Leipzig)* **5**, 224 (1996).
- ¹⁴J. M. Tranquada, D. J. Buttrey, V. Sachan, and J. E. Lorenzo, *Phys. Rev. Lett.* **73**, 1003 (1994); J. M. Tranquada, J. E. Lorenzo, D. J. Buttrey, and V. Sachan, *Phys. Rev. B* **52**, 3581 (1995).
- ¹⁵J. Zaanen and P. B. Littlewood, *Phys. Rev. B* **50**, 7222 (1994).
- ¹⁶T. Mizokawa and A. Fujimori, *Phys. Rev. B* **56**, 11920 (1997).
- ¹⁷A. M. Oleś, *Acta Phys. Pol. B* **31**, 2963 (2000).
- ¹⁸S. I. Matveenko and S. I. Mukhin, *Phys. Rev. Lett.* **84**, 6066 (2000).
- ¹⁹G. Seibold, E. Sigmund, and V. Hizhnyakov, *Phys. Rev. B* **57**, 6937 (1998); G. Seibold, C. Castellani, C. Di Castro, and M. Grilli, *ibid.* **58**, 13506 (1998).
- ²⁰S. R. White and D. Scalapino, *Phys. Rev. Lett.* **80**, 1272 (1998); **81**, 3227 (1998).
- ²¹D. Góra, K. Rościszewski, and A. M. Oleś, *Phys. Rev. B* **60**, 7429 (1999).
- ²²C. Buhler, S. Yunoki, and A. Moreo, *Phys. Rev. Lett.* **84**, 2690 (2000).
- ²³P. Wróbel and R. Eder, *Int. J. Mod. Phys. B* **14**, 3765 (2000).
- ²⁴M. Fleck, A. I. Lichtenstein, E. Pavarini, and A. M. Oleś, *Phys. Rev. Lett.* **84**, 4962 (2000).
- ²⁵G. Stollhoff and P. Thalmeier, *Z. Phys. B* **43**, 13 (1981); A. M. Oleś, *Phys. Rev. B* **23**, 271 (1981).
- ²⁶K. Yamada, C. H. Lee, K. Kurahashi, J. Wada, S. Wakimoto, S. Ueki, H. Kimura, Y. Endoh, S. Hosoya, G. Shirane, R. J. Birgeneau, M. Greven, M. A. Kastner, and Y. J. Kim, *Phys. Rev. B* **57**, 6165 (1998).
- ²⁷A. Georges, G. Kotliar, W. Krauth, and M. J. Rozenberg, *Rev. Mod. Phys.* **68**, 13 (1996).
- ²⁸W. Metzner and D. Vollhardt, *Phys. Rev. Lett.* **62**, 324 (1989).
- ²⁹M. Fleck, A. I. Lichtenstein, A. M. Oleś, L. Hedin, and V. I. Anisimov, *Phys. Rev. Lett.* **80**, 2393 (1998).
- ³⁰M. Fleck, A. I. Lichtenstein, and A. M. Oleś, in *High Temperature Superconductivity*, edited by S. E. Barnes, J. Ashkenazi, J. L. Cohn, and F. Zuo, AIP Conf. Proc. No. 483 (AIP, New York, 2000), p. 45.
- ³¹M. Caffarel and W. Krauth, *Phys. Rev. Lett.* **72**, 1545 (1994).
- ³²S. Wakimoto, G. Shirane, Y. Endoh, K. Hirota, S. Ueki, K. Yamada, R. J. Birgeneau, M. A. Kastner, Y. S. Lee, P. M. Gehring, and S. H. Lee, *Phys. Rev. B* **60**, 769 (1999); S. Wakimoto, R. J. Birgeneau, M. A. Kastner, Y. S. Lee, R. Erwin, P. M. Gehring, S. H. Lee, M. Fujita, K. Yamada, Y. Endoh, K. Hirota, and G. Shirane, *ibid.* **61**, 3699 (2000).
- ³³J. H. Jefferson, H. Eskes, and L. F. Feiner, *Phys. Rev. B* **45**, 7959 (1992); L. F. Feiner, J. H. Jefferson, and R. Raimondi, *ibid.* **53**, 8751 (1996).
- ³⁴O. K. Andersen, A. I. Lichtenstein, O. Jepsen, and F. Paulsen, *J. Phys. Chem. Solids* **56**, 1573 (1995).
- ³⁵H.-H. Klauss, W. Wagener, M. Hillberg, W. Kopmann, H. Walf, F. J. Litterst, M. Hücker, and B. Büchner, *Phys. Rev. Lett.* **85**, 4590 (2000).
- ³⁶A. Ino, T. Mizokawa, A. Fujimori, K. Tamasaku, H. Eisaki, S. Uchida, T. Kimura, T. Sasagawa, and K. Kishio, *Phys. Rev. Lett.* **79**, 2101 (1997).
- ³⁷A. Ino, C. Kim, T. Mizokawa, Z. X. Shen, A. Fujimori, M. Takaba, K. Tamasaku, H. Eisaki, and S. Uchida, *J. Phys. Soc. Jpn.* **68**, 1496 (1999).
- ³⁸Z.-X. Shen, W. E. Spicer, D. M. King, D. S. Dessau, and B. O. Wells, *Science* **267**, 343 (1995).
- ³⁹X. J. Zhou, P. Bogdanov, S. Kellar, T. Noda, H. Eisaki, S. Uchida, Z. Hussain, and Z.-X. Shen, *Science* **286**, 268 (1999).
- ⁴⁰R. S. Markiewicz, *Phys. Rev. B* **62**, 1252 (2000).
- ⁴¹P. Wróbel and R. Eder, *Phys. Rev. B* **62**, 4048 (2000).
- ⁴²M. G. Zacher, R. Eder, E. Arrigoni, and W. Hanke, *Phys. Rev. Lett.* **85**, 2585 (2000).
- ⁴³J. Eroles, G. Ortiz, A. V. Balatsky, and A. R. Bishop, *Europhys. Lett.* **50**, 540 (2000); cond-mat/0008341, *Phys. Rev. B* (to be published).
- ⁴⁴M. Moraghebi, C. Buhler, S. Yunoki, and A. Moreo, *Phys. Rev. B* **63**, 214513 (2001).
- ⁴⁵A. Ino, C. Kim, M. Nakamura, T. Yoshida, T. Mizokawa, Z. X. Shen, A. Fujimori, T. Kakeshita, H. Eisaki, and S. Uchida, *Phys. Rev. B* **62**, 4137 (2000).
- ⁴⁶M. Potthoff and W. Nolting, *Eur. Phys. J. B* **8**, 555 (1999).
- ⁴⁷M. Fleck, A. I. Lichtenstein, A. M. Oleś, and L. Hedin, *Phys. Rev. B* **60**, 5224 (1999).
- ⁴⁸D. Vollhardt, in *Correlated Electron Systems*, edited by V. J. Emery (World Scientific, Singapore, 1993), p. 57.
- ⁴⁹S. Wakimoto, S. Ueki, Y. Endoh, and K. Yamada, *Phys. Rev. B* **62**, 3547 (2000).
- ⁵⁰M. Bosch, W. van Saarloos, and J. Zaanen, *Phys. Rev. B* **63**, 092501 (2001).
- ⁵¹P. Prelovšek and X. Zotos, *Phys. Rev. B* **47**, 5984 (1993); P. Prelovšek and I. Sega, *Phys. Rev. B* **49**, 15 241 (1994).
- ⁵²V. J. Emery, S. A. Kivelson, and H. Q. Lin, *Phys. Rev. Lett.* **64**, 475 (1990).
- ⁵³E. S. Božin, G. H. Kwei, H. Takagi, and S. Billinge, *Phys. Rev. Lett.* **84**, 5856 (2000).
- ⁵⁴L. Chen, C. Bourbonnais, T. Li, and A.-M. S. Tremblay, *Phys. Rev. Lett.* **66**, 369 (1991); Y. M. Vilks and A.-M. S. Tremblay, *J. Phys. I* **7**, 1309 (1997).
- ⁵⁵M. Fleck, A. M. Oleś, and L. Hedin, *Phys. Rev. B* **56**, 3159 (1997).
- ⁵⁶G. Martínez and P. Horsch, *Phys. Rev. B* **44**, 317 (1991).
- ⁵⁷S. Schmitt-Rink, C. M. Varma, and A. E. Ruckenstein, *Phys. Rev. Lett.* **60**, 2793 (1989).
- ⁵⁸P. Wróbel and R. Eder, *Int. J. Mod. Phys. B* **14**, 3759 (2000).
- ⁵⁹H. Eskes and A. M. Oleś, *Phys. Rev. Lett.* **73**, 1279 (1994); H. Eskes, A. M. Oleś, M. Meinders, and W. Stephan, *Phys. Rev. B* **50**, 17980 (1994).
- ⁶⁰For a review, see J. Jaklič and P. Prelovšek, *Adv. Phys.* **49**, 1 (2000).
- ⁶¹E. Dagotto, *Rev. Mod. Phys.* **66**, 763 (1994).
- ⁶²A. Ramšak and P. Horsch, *Phys. Rev. B* **57**, 4308 (1998).
- ⁶³L. Hedin, *J. Phys.: Condens. Matter* **11**, 489 (1999).
- ⁶⁴T. Timusk and B. Statt, *Rep. Prog. Phys.* **62**, 61 (1999).
- ⁶⁵M. Momono, M. Ido, T. Nakano, M. Oda, Y. Okajima, and K. Yamaya, *Physica C* **233**, 395 (1994).
- ⁶⁶M. Fleck, E. Pavarini, and O. K. Andersen, cond-mat/0102041 (unpublished).
- ⁶⁷J. Bała, A. M. Oleś, and J. Zaanen, *Phys. Rev. B* **52**, 4597 (1995);

- P. W. Leung, B. O. Wells, and R. J. Gooding, *ibid.* **56**, 6320 (1997); R. Eder, Y. Ohta, and G. A. Sawatzky, *ibid.* **55**, R3414 (1997); O. P. Sushkov, G. A. Sawatzky, R. Eder, and H. Eskes, *ibid.* **56**, 11769 (1997); J. van den Brink and O. P. Sushkov, *ibid.* **57**, 3518 (1998).
- ⁶⁸Z.-X. Shen and J. R. Schrieffer, Phys. Rev. Lett. **78**, 1771 (1997); C. Kim, P. J. White, Z.-X. Shen, T. Tohyama, Y. Shibata, S. Maekawa, B. O. Wells, Y. J. Kim, R. J. Birgeneau, and M. A. Kastner, *ibid.* **80**, 4245 (1998).
- ⁶⁹B. Normand and A. P. Kampf, Phys. Rev. B **64**, 024521 (2001).
- ⁷⁰C. Gröber, R. Eder, and W. Hanke, Phys. Rev. B **62**, 4336 (2000).
- ⁷¹D. S. Dessau, T. Saitoh, C.-H. Park, Z.-X. Shen, P. Villella, N. Hamada, Y. Moritomo, and Y. Tokura, Phys. Rev. Lett. **81**, 192 (1998).
- ⁷²A. Moreo, S. Yunoki, and E. Dagotto, Phys. Rev. Lett. **83**, 2773 (1999).
- ⁷³N. Furukawa and M. Imada, J. Phys. Soc. Jpn. **62**, 2557 (1993).
- ⁷⁴N. Bulut, D. J. Scalapino, and S. R. White, Phys. Rev. B **47**, 2742 (1993).
- ⁷⁵L. F. Feiner, J. H. Jefferson, and R. Raimondi, Phys. Rev. Lett. **76**, 4939 (1996); R. Raimondi, J. H. Jefferson, and L. F. Feiner, Phys. Rev. B **53**, 8774 (1996); E. Pavarini, I. Dasgupta, T. Saha-Dasgupta, O. Jepsen, and O. K. Andersen, Phys. Rev. Lett. **87**, 047003 (2001).
- ⁷⁶A. Sadori and M. Grilli, Phys. Rev. Lett. **84**, 5375 (2000).
- ⁷⁷T. Senthil and M. Fisher, Phys. Rev. B **61**, 9690 (2000); Phys. Rev. Lett. **86**, 292 (2001).